Analysis of the DNA damage signal transducer ortholog *Mop53BP1* in *Pyricularia oryzae*

(イネいもち病菌の DNA 損傷トランスデューサーオーソログ Mop53BP1 の解析)

Hokkaido University Graduate School of Agriculture

Division of Bio-systems Sustainability Doctor Course

Andre Ohara

TABLE OF CONTENTS

Table of contents..……...i

List of tables…….....iv

List of figures…….v

List of appendices…….ix

CHAPTER ONE 1

1. General Overview 2

1.1. The blast fungus 2

1.2. Cell cycle regulation of appressorium development in *P. oryzae* 3

1.3. The signal transducer p53 binding protein 1 (*53BP1*) 7

1.4. The ortholog *Mop53BP1* in *P. oryzae* 8

1.5. Objectives 13

CHAPTER TWO 14

2. Expression analysis of *Mop53BP1* 15

2.1. Expression analysis of *Mop53BP1* in the presence of DNA damage agents..... 15

2.1.1. DNA damage treatments for gene expression study 15

2.2.2. RNA extraction and qRT-PCR reaction..... 16

2.2. Cellular localization and expression of Mop53BP1 in P. oryzae 19

2.2.1. Construction of pBLASTR-DEST-P$_{Mop53BP1}$::eGFP::*Mop53BP1* plasmid... 19

2.2.2. Fungal transformation 20

2.2.3. Screening of mutants by PCR and Southern Hybridization 22

2.2.4. Appressorium induction and evaluation of *Mop53BP1* expression during appressorium formation..... 23

CHAPTER THREE..... 31

3. Overexpression of *Mop53BP1* and interaction with other proteins…….. 32

3.1. Construction of overexpression mutants..... 32

3.1.1 Construction of pBLASTR-DEST-TEF::eGFP::Mop53BP1 plasmid and transformation 32

3.1.2. Appressorium induction using onion epidermis membrane and evaluation of *Mop53BP1* overexpression 35

3.2. Interaction of Mop53BP1 with proteins related to cell cycle progression……...42

3.2.1. Monitoring the influence of Mop53BP1 in the cell cycle progression by using an inhibitor of DNA synthesis HU and the microtubule inhibitor benomyl. 42

3.3. Evaluating the relationship between Mop53BP1 and the microtubule inhibitor benomyl 46

3.3.1. *Mop53BP1* deletion and overexpression mutants exposed to benomyl..... 46

CHAPTER FOUR 53

4. Visualization and expression of α-Tubulin in *P. oryzae* deletion mutants..... 54

4.1. Evaluating the relationship between Mop53BP1 and α-Tubulin..... 54

4.1.1. Construction of pBLASTR-DEST-TEF::mCherry::Tuba plasmid and transformation 54

4.1.2. Appressorium induction using hydrophobic microscope glass slides..... 56

CHAPTER FIVE 62

Summary 62

CHAPTER SIX 67

References.....67

Appendices.....73

List of abbreviations.....88

Acknowledgements 90

LIST OF TABLES

Table 1. Synthetic oligonucleotides used in the expression analysis and localization of Mop53BP1. ……30

Table 2. Synthetic oligonucleotides used in the overexpression of Mop53BP1. ……52

Table 3. Synthetic oligonucleotides used in the expression of α-Tubulin tagged to mCherry in *P. oryzae*…...……..……...……61

LIST OF FIGURES

Figure 1. Blast lesions on leaf and spike. (a) Diamond-shaped lesions on leaf (b) Infection in the rachis killing the upper parts of the spike……..3

Figure 2. Life cycle of the rice blast fungus *Pyricularia oryzae*……4

Figure 3. Schematic diagram of the appressorium development controlled by the cell cycle progression……...6

Figure 4. DNA damage response pathways in mammals……...……...8

Figure 5. Schematic presentation of Mop53BP1 in *Pyricularia oryzae.* (a) Protein alignment between *Mop53BP1* in *P. oryzae*, human and mouse 53BP1, *S. pombe* Crb2 and *C. elegans* HSR-9 showing each size and identity to Mop53BP1. The position of Tudor domains and BRCA domains are presented. (b) Clustalw comparing C-terminal BRCT domains, * indicates positions which have a single, fully conserved residue, : indicates conservation between groups of strongly similar properties and · indicates conservation between groups of weakly similar properties……..10

Figure 6. Wild-type (WT) Ina 168 and 86-137, and deletion mutants grown from 10 days on PA medium supplemented with DNA damage agents MMS and H_2O_2……...11

Figure 7. Appressorium formation and pathogenicity of wild-type, *ΔMop53BP1* and complementation mutants. (a) Appressorium abnormalities presented by *ΔMop53BP1* mutants. (b)Wild-type, complementation and deletion mutants average number of appressorium per conidia. (c) Histone-GFP showing a higher proportion of germinated conidia lacking nuclear autophagy after appressorium formation in *ΔMop53BP1*. (d) *ΔMop53BP1* mutant inoculated on to intact leaf sheath. Microscopic observations were

performed after 48 h. Scale bar = 5 μm, SP; conidia, AP; appressoria, and IH, invasive hyphae. (e) Symptom of rice leaf Spray-inoculated with Ina168 wild-type (WT), *ΔMop53BP1* mutant Δ2, and complementation strain Δ2com9……12

Figure 8. Expression analyzes of Mop53BP1 exposed to different DNA damage treatments. (a) RT-PCR for *Mop53BP1* amplification after DNA damage treatments. 1-1KB ladder, 2-Control, 3-HS, 4-HU, 5-MV, 6-MMS. (b) Real-time PCR results for *Mop53BP1* expression in the presence of DNA damage agents HU, MV, MMS, and heat shock, after grown on 2YEG medium for 3 days. The expression of *Rhm51* (*RAD51* homolog) was evaluated as a positive control……...18

Figure 9. Construction of pBLASTR-DEST-P$_{Mop53BP1}$::eGFP::*Mop53BP1* plasmid. After inverse PCR and LR-clonase reaction steps, the destination vector was linearized with *PsiI* and used to transform INA86-137 *Mop53BP1* disruption mutants……...21

Figure 10. Confirmation of positive transformants and expression of the GFP-Mop53BP1 construct. (a) PCR performed with primers eGFPF and Mop53BP1R (Table 1), and Southern hybridization by digesting genomic DNA with Hind III and EcoRI and using eGFP fragment as a probe. (b) Expression of the GFP-Mop53BP1 fusion under the control of the native promoter during appressorium formation. Scale bar = 5 μm……25

Figure 11. Expression analyzes of Mop53BP1 during the first hours of appressorium formation (a) RT-PC and (b) qRT-PC for *Mop53BP1* expression during 0h, 3h, 6h and 9h of appressorium development…….27

Figure 12. Construction of pBLASTR-DEST-TEF::eGFP::*Mop53BP1* plasmid. The destination vector was linearized with *PsiI* and used to transform INA86-137 *Mop53BP1* wild-type and disruption mutants…….34

Figure 13. Confirmation of positive transformants. PCR performed with primers TEF-GFPfw and 53BP12R (Table 2), and Southern hybridization by digesting genomic DNA with KpnI and EcoRI and using eGFP fragment as a probe……..36

Figure 14. Expression of the GFP-Mop53BP1 fusion under the control of TEF1 promoter during appressorium formation. Strong green fluorescence was observed in the nuclei regions of cells on glass slides surface. Scale bar = 5 μm……..39

Figure 15. Expression of the GFP-Mop53BP1 fusion under the control of TEF1 promoter during appressorium formation and onion epidermis infection. Fluoresce exhibit the same pattern during all steps of plant infection and signals were also detected after invasive hyphae formation. Scale bar = 5 μm…….40

Figure 16. Comparison between vegetative growth of wild-type, *ΔMop53BP1* and overexpression mutants in 2YEG medium during 24 hours. No significant difference between strains growth was observed. Scale bar = 5 μm……..41

Figure 17. Scheme showing cell-cycle transitions necessary for appressorium-mediated plant infection by *M. oryzae*, indicating the target region for HU and Benomyl action…42

Figure 18. Appressoria development under exposure to HU and benomyl. (a) Appressorium formation by WT (control observed after 12 h) and *ΔMop53BP1* mutant following exposure to 200 mM HU, observed at 24 h. (b) Appressorium formation by WT (control observed after 12 h), *ΔMop53BP1*mutant and WT following exposure to benomyl (5 mg/mL^{-1}), observed at 24 h. Scale bar = 5 μm…….....45

Figure 19. Appressorium development of wild-type and *ΔMop53BP1*mutant exposed to different concentrations of the microtubule inhibitor benomyl. Deletion mutant showed hypersensitivity to the microtubule inhibitor in all assays forming abnormal and multiple

appressoria. Wild-type could develop normal appressorium in the lowest concentration of benomyl. Scale bar = 5 μm……...48

Figure 20. Effect of Benomyl on appressoria development. Overexpression mutant presented some resistance to benomyl following exposure to 5 mg/mL, observed at 0h, 6h, and 12h……...49

Figure 21. Effect of Benomyl on appressoria development. WT development following exposure to benomyl (5 mg/mL−1), observed at 12 h and 24 h. Scale bar = 5 μm…….50

Figure 22. Construction of pBLASTR-DEST-TEF::mCherry::Tuba plasmid. The destination vector was linearized with *PsiI* and used to transform INA86-137 *Mop53BP1* wild-type and disruption mutants…….55

Figure 23. Confirmation of positive transformants by PCR and Southern hybridization. PCR with primers RFPovf and RFPovr (Table 2), and Southern hybridization by digesting genomic DNA with PsiI and EcoRI and using mCherry fragment as a probe……...57

Figure 24. Expression of the mCherry-αTubulin fusion under the control of TEF1 promoter during appressorium formation of the wild-type strain. Fluorescence observed after 6 hours of growth. Scale bar = 5 μm…….58

Figure 25. Expression of the mCherry-αTubulin fusion under the control of TEF1 promoter during appressorium formation of *ΔMop53BP1* strain. Fluorescence signals were undetected during all steps of appressorium development. Scale bar = 5 μm……..59

LIST OF APPENDICES

APPENDIX I: Reaction conditions and composition of solutions……75

APPENDIX II: DNA damage agents, antibiotics, and fungicidal compounds used in this study…….87

CHAPTER ONE

General Overview

Chapter 1

1. General Overview

1.1. The blast fungus

Pyricularia oryzae (teleomorph: *Magnaporthe oryzae*) is the causal agent of the rice blast, the most important disease that affects rice production worldwide. Rice blast has been causing epidemics in all rice-growing regions, and this disease is extremely difficult to control (Wilson and Talbot 2009). Since more than half of the global population depends on rice as a staple food crop, rice blast disease represents a significant factor that impacts upon global food security (Soanes et al. 2012). Recently, the blast fungus emerged as an explosive threat to wheat production that can cause 100% yield losses. The wheat blast was observed for the first time in 1985 in South America and last year the disease devastated wheat crops in Bangladesh. The most common and diagnostic symptom of blast disease are diamond-shaped lesions on the leaves (Fig. 1a) however the most visible symptom of wheat blast in the fields is bleaching of the spike (Fig. 1b) (Cruz and Valent 2017). Until now, the chemical control and the incorporation of resistant (R) genes into host plants are the most effective and economical strategies to control blast. However, the fungus can overcome the effect of R genes within 2 or 3 years after planting and can develop fungicide resistance (Wang and Valent 2017; Cruz and Valent 2017). Taking into consideration that it takes years to move an R gene into a rice variety, and the extensive use of fungicides led to a widespread distribution of mutations conferring resistance in *Pyricularia* strains, a better understanding of infection process, fungi-host interaction and plant resistance mechanisms are necessary in an attempt to reduce the damages caused by this disease.

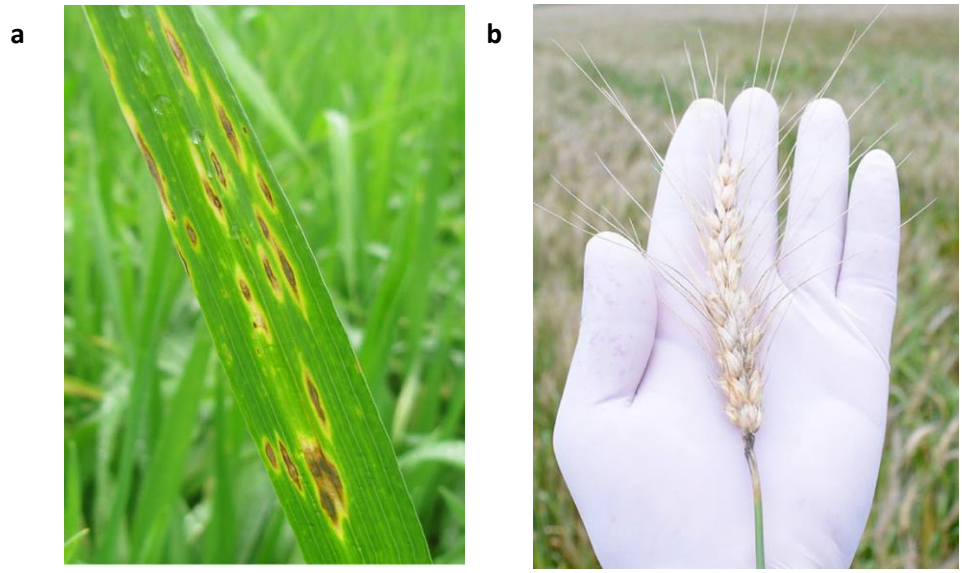

Figure 1. Blast lesions on leaf and spike. (a) Diamond-shaped lesions on leaf (b) Infection in the rachis killing the upper parts of the spike (Cruz and Valent 2017).

1.2. Cell cycle regulation of appressorium development in P. oryzae

Similar to other pathogenic fungi (*Puccinia* sp., *Colletotrichum* sp, *Ustilago maydis*, *Phakopsora pachyrhizi*, *Fusarium* sp., *Botrytis cinereal*, etc), *P. oryzae* develops a specialized structure called appressoria (Ludwig et al. 2014; Lanver et al. 2014; Chang et al. 2014; Schamber et al. 2010; Jenczmionka et al. 2003) (Fig. 2). The appressorium formation starts as soon as a spore lands on the leaf surface, after that there are a set of several inductive cues of extracellular nature (environmental signals as waxy leaf cuticle and perception of hydrophobicity), while others are intracellular (developmental signals controlled by the cell cycle) (Kou and Naqvi 2016; Franck et al. 2013). The appressoria morphology is variable according to the pathogenic fungi, however all appressoria formation requires cell modifications which are ruled by the cell cycle progress.

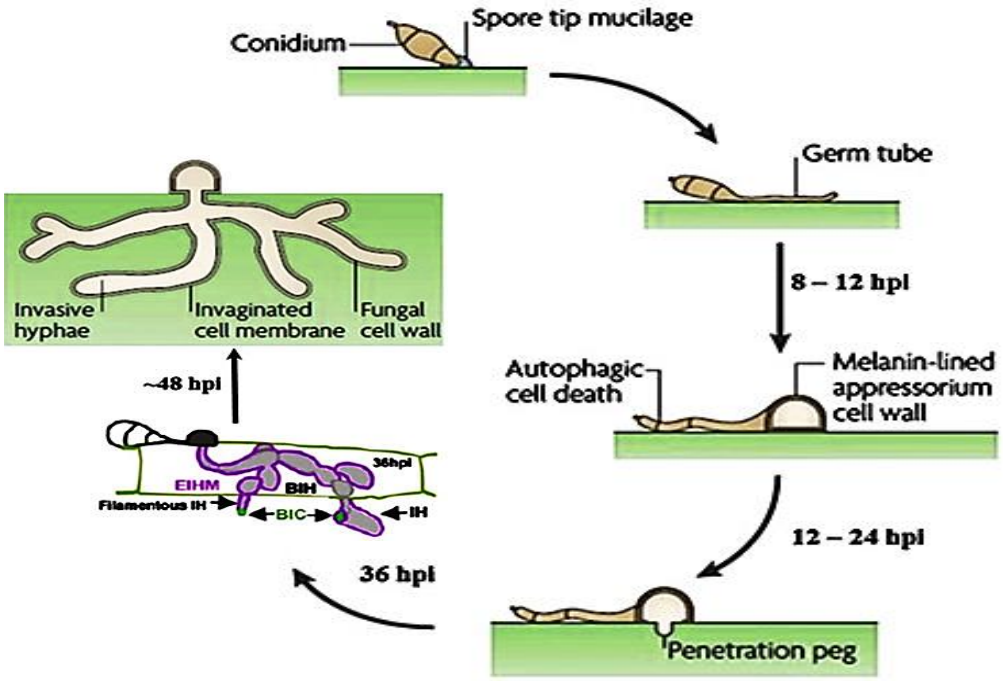

Figure 2. Life cycle of the rice blast fungus *Pyricularia oryzae* (Donofrio et al. 2014).

After attaching to the host plant surface, one of the cells composing the three-celled conidium starts to germinate. During this step, a germ tube is produced from a single nucleus at G1. Then after s-phase completion, a germ tube emerges extending for 10–15 μm. Once the germ tube reaches the proper size, the cell enters the G2 phase. Subsequently, the appressorium expands and in order to mature, the cell nucleus enters mitosis. The maturation process involves the melanization of appressorium, which generates osmotic pressure by accumulation of glycerol and applies mechanical pressure to breach the leaf surface, growing invasively into the first epidermal cells by means of invasive hyphae (Wilson and Talbot 2009; Ryder and Talbot 2015; Pérez-Martin et al. 2016) (Fig. 3).

Therefore, the cell cycle is crucial to cellular differentiation in multicellular eukaryotes, which must synchronize cell division to form specific tissues and organs effectively. During the last years, it was evidenced that cell cycle regulation provides control points for infection structure development in *P. oryzae*. It was also demonstrated that proper mitosis is necessary for appressorium formation and followed by conidial autophagy, which is essential for the successful plant infection (Fig. 3).

The key steps for the initiation and completion of appressorium formation in *P. oryzae* are the entry into S-phase and mitosis. According to Saunders et al. (2010), the initial appressorium development is directly dependent on a successful DNA replication. After that, the mitotic entry is necessary and sufficient to start the appressorium maturation in *P. oryzae,* and finally, the exit from mitosis appears to be required for plant infection. Also, another interesting characteristic is that the differentiation of appressoria requires a cytokinetic event that is distinct from cell divisions within hyphae.

Although the relationship between cell cycle and appressorium formation has been extensively studied during the last years, the protein factors working in DNA damage checkpoints, whose roles in cell cycle control are well elucidated in higher eukaryotes, still not been well characterized in *P. oryzae* and other pathogenic fungi.

Moreover, according to Ndindeng et al. (2010), *P. oryzae* suffers double-strand DNA break during multiples stages in its life cycle including appressorium formation. Therefore, the analysis of factors working in response to DNA damage during appressorium formation should provide us valuable information on the pathogenesis of *P. oryzae.*

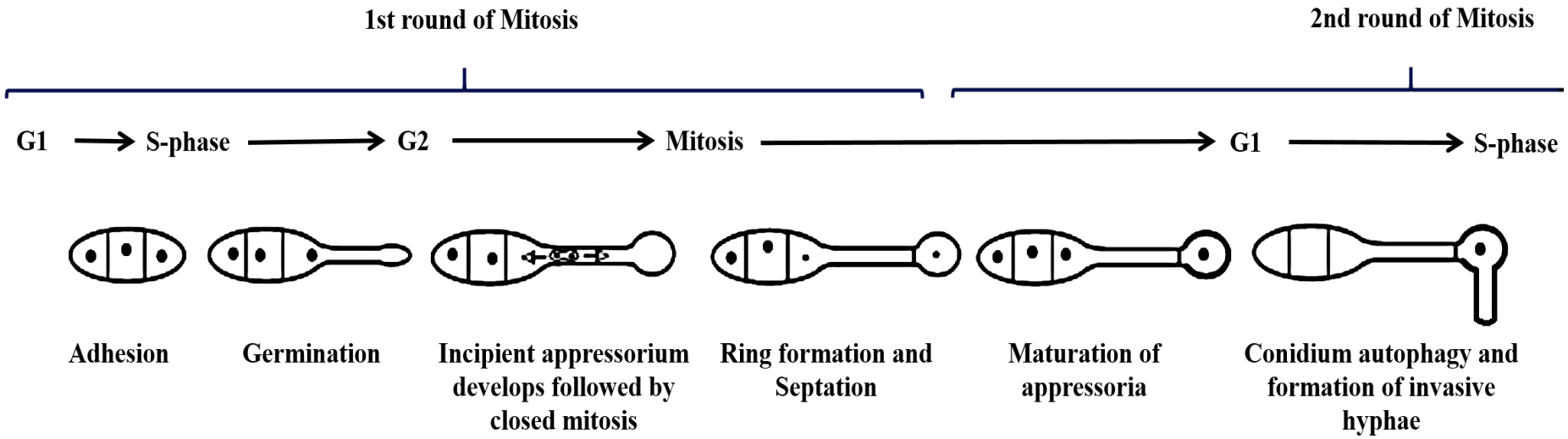

Figure 3. Schematic diagram of the appressorium development controlled by the cell cycle progression (Saunders et al. 2010).

1.3. The signal transducer p53 binding protein 1 (53BP1)

The gene *TP53* was the first tumor suppressor gene to be identified since half of the human tumors possess mutations, which inactivates this gene. The protein (p53) plays a major role in the cellular proliferation control, in some occasions stopping the cell cycle in G1 checkpoint phase, allowing DNA repair, and sometimes promoting apoptosis, when the damages cannot be repaired (Olivier et al. 2010). Another tumor suppressor gene is *53BP1*, which is also an important regulator of the genomic stability, acting on cellular response to double-strand DNA break repair. The protein p53BP1 interacts with the central region of the protein p53, and the inactivation of this gene is associated with a higher tumor predisposition development caused by a high sensitivity to ionizing radiation (Panier and Boulton 2014; Jullien et al. 2002). DNA damage response pathways, sensors, mediators, effectors, and transducers are shown in figure 4.

53BP1 and orthologs Crb2 and HSR-9 play important roles in many cellular processes, including DNA damage, cell cycle checkpoint arrests, apoptosis and also a form of nonhomologous end-joining (NHEJ). In regards to DNA damaging agents, 53BP1 regulates p53 and Chk2 (Checkpoint kinase 2) in response to ionizing radiation, being a critical transducer of the DNA damage signal and is required for both the intra-S-phase and G2-M checkpoints (Wang et al. 2002; Fernandez-Capetillo et al. 2002). In addition, according to Rappold et al. (2001), 53BP1 becomes hyperphosphorylated and forms nuclear foci in response to DNA damage treatments as γ-irradiation, UV, -nitroquinoline 1-oxide (4NQO), hydroxyurea, camptothecin, etoposide, MMS, cisplatin, 7-hydroxystaurosporine, and paclitaxel. A similar sensibility is observed in the ortholog Crb2 from *S. pombe*. Crb2 is required for checkpoint arrests induced by irradiation and polymerase mutations (Saka et al. 1997). The 53BP1 homolog in *C. elegans* HSR-9 is not

directly involved in cell cycle arrest however it promotes apoptosis in response to ionizing radiation.

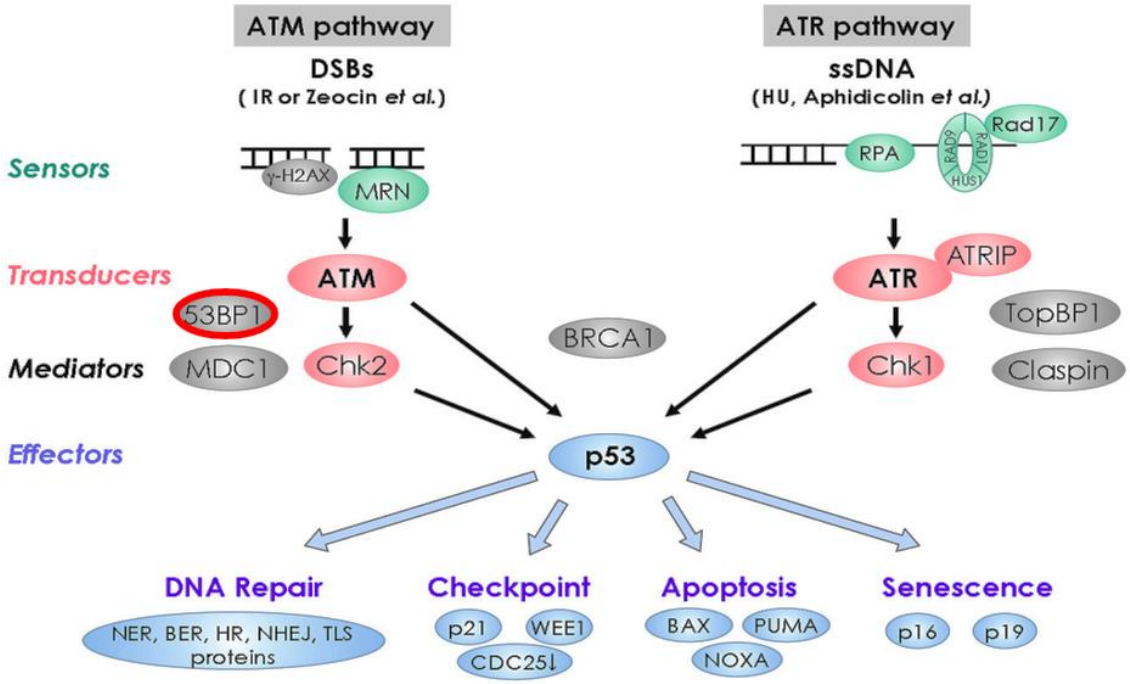

Figure 4. DNA damage response pathways in mammals (Yoshiyama et al. 2013).

1.4. The ortholog Mop53BP1 in P. oryzae

In previous studies (Tashika et al. unpublished data), an ortholog *Mop53PB1* was identified in the *P. oryzae* pathogen. By carrying out a BLAST search of the *P. oryzae* ORFs, an uncharacterized protein (MGG_12276) of 1015 aa - that had 19% amino acid identity with human and mouse p53BP1, 23% identity with HSR-9 from *C. elegans* and 22% with Crb2 from *S. pombe* was identified (Fig. 1). Considering important regions and domains found during the BLAST search, the Tudor domain is present in human and mouse p53BP1 as well as in Crb2 from *S. pombe*; this domain contains a region responsible for recognition of histone H4 in DNA repair (Botuyan et al. 2006). In addition, when all species were compared, the identity was found mainly in the C-terminal BRCT

region, which is observed as tandem in human and mouse and single in *S. pombe*, *C. elegans* and *P. oryzae* (Fig. 5a and 5b). The BRCT, an evolutionary conserved protein-protein interacting domain, has been observed as single, tandem or multiple repeats in several proteins with functions related to the DNA-damage response (Derbyshire et al. 2002) Although Mop53BP1 is not the only one protein with BRCT region in *P. oryzae*, it is well known that p53BP1 is a conserved nuclear protein involved in the DNA damage response (DiTullio et al. 2002).

Therefore, for a better understanding of the physiological function of *Mop53BP1* in *P. oryzae*, a gene disruption strategy was adopted. *ΔMop53BP1* mutants showed no significant difference in vegetative growth on Prune Agar medium (PA) when compared to the wild-type strain and complemented strains, even on the media containing the DNA damaging agents H_2O_2 and Methyl methanesulfonate (MMS) (Fig. 6). However, deletion mutants presented abnormalities in appressorium formation; the number of appressoria per conidia was higher than wild-type (Fig. 7a and 7b). Nuclear dynamics in appressorium differentiation, visualized by histone-EGFP, revealed a higher proportion of germinated conidia lacking nuclear autophagy after the first appressorium formation (Fig. 7c) (Tashika et al. unpublished data).

In addition, wild-type strain and complementation mutants were able to develop proper appressorium and caused visible disease symptoms on rice (Fig. 7e), despite forming few normal appressoria structures, deletion mutants mostly developed more than one appressoria per conidia (Fig. 7d), and consequently reduced in virulence (Fig. 7e) (Tashika et al. unpublished data).

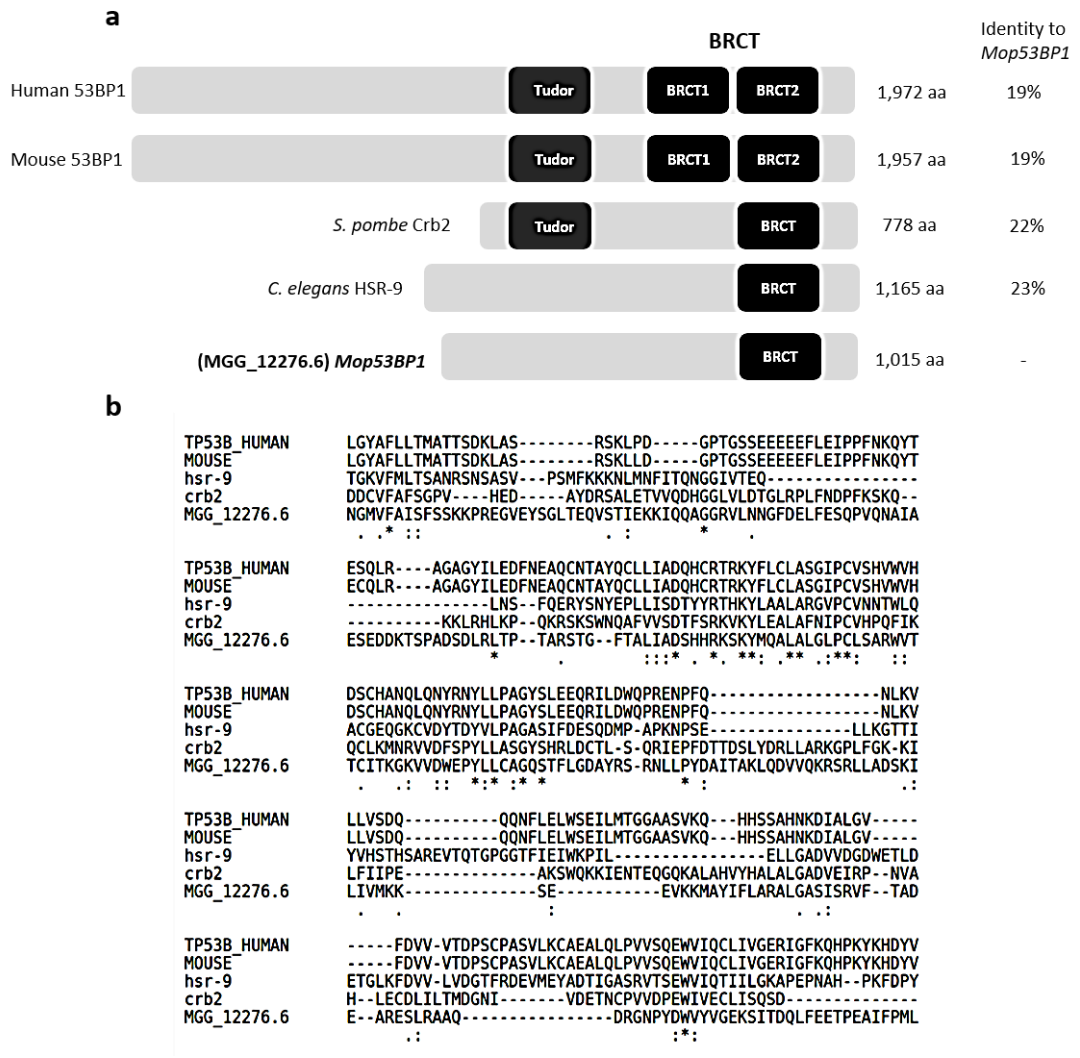

Figure 5. Schematic presentation of Mop53BP1 in *Pyricularia oryzae*. (a) Protein alignment between *Mop53BP1* in *P. oryzae*, human and mouse 53BP1, *S. pombe* Crb2 and *C. elegans* HSR-9 showing each size and identity to Mop53BP1. The position of Tudor domains and BRCA domains are presented. (b) Clustalw comparing C-terminal BRCT domains, * indicates positions which have a single, fully conserved residue, : indicates conservation between groups of strongly similar properties and · indicates conservation between groups of weakly similar properties.

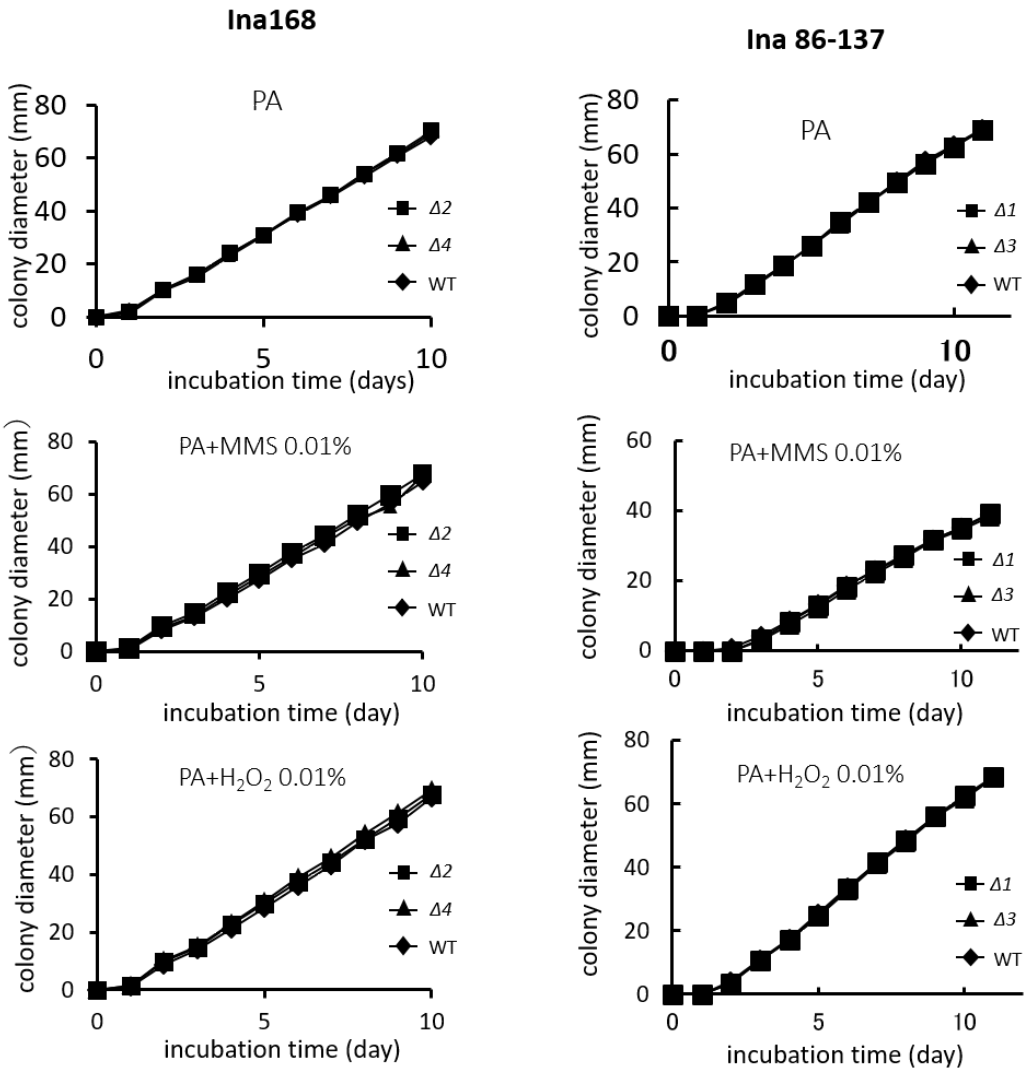

Figure 6. Wild-type (WT) Ina 168 and 86-137, and deletion mutants grown from 10 days on PA medium supplemented with DNA damage agents MMS and H_2O_2 (Tashika et al. unpublished data).

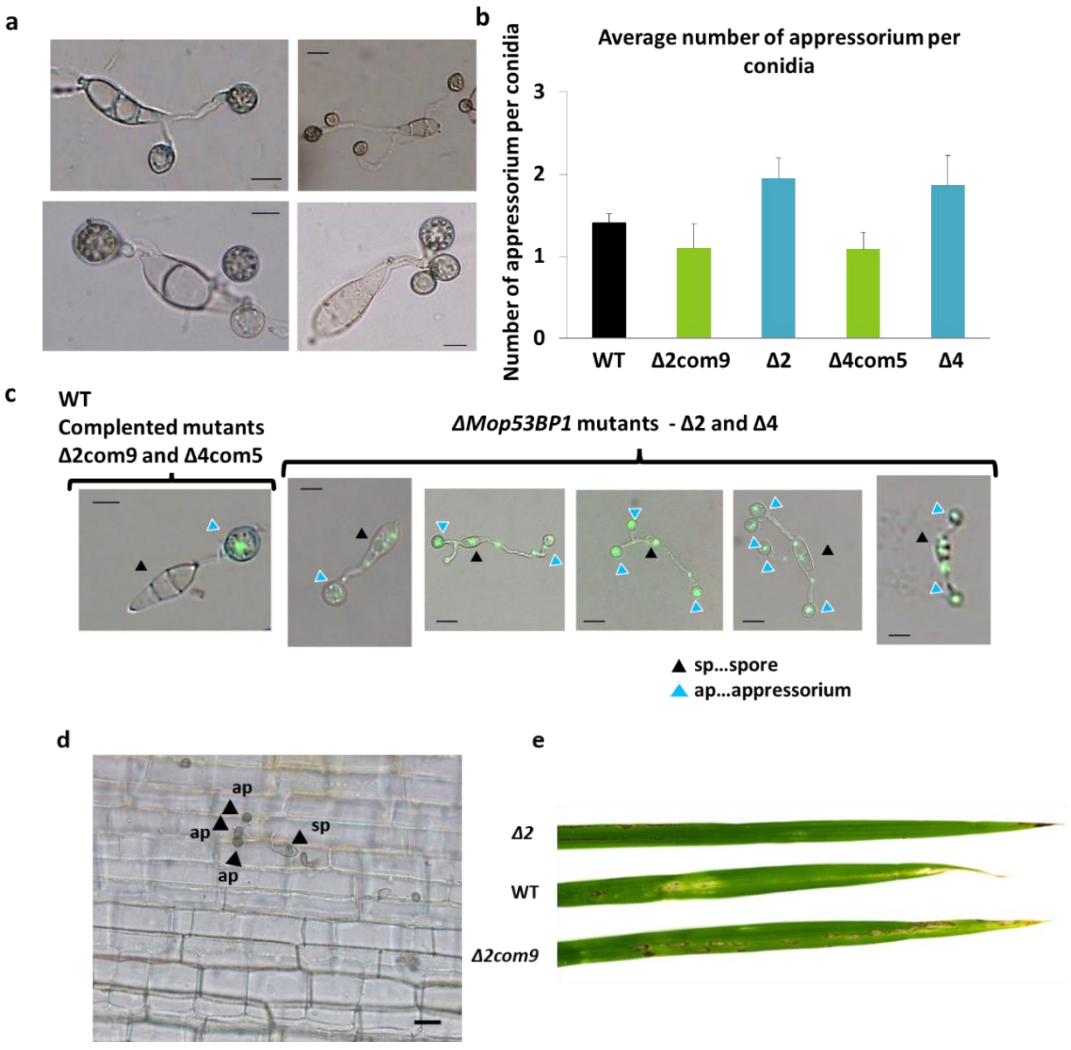

Figure 7. Appressorium formation and pathogenicity of wild-type, *ΔMop53BP1* and complementation mutants. (a) Appressorium abnormalities presented by *ΔMop53BP1* mutants. (b)Wild-type, complementation and deletion mutants average number of appressorium per conidia. (c) Histone-GFP showing a higher proportion of germinated conidia lacking nuclear autophagy after appressorium formation in *ΔMop53BP1*. (d) *ΔMop53BP1* mutant inoculated on to intact leaf sheath. Microscopic observations were performed after 48 h. Scale bar = 5 µm, SP; conidia, AP; appressoria, and IH, invasive hyphae. (e) Symptom of rice leaf Spray-inoculated with Ina168 wild-type (WT), *ΔMop53BP1* mutant Δ2, and complementation strain Δ2com9 (Tashika et al. unpublished data).

1.5. Objectives

The rice blast disease caused by the fungus *P. oryzae* is considered the most devastating disease of rice worldwide, and recently demonstrated the threat of global spread also in wheat plantations. In order to penetrate the host plant, *P. oryzae* develops an appressorium structure, which is one of the most important steps in the pathogenesis of blast fungus.

A strong relationship between appressorium differentiation and cell cycle had been found in *P. oryzae*, and genes involved in this process demonstrated to be essential for the appressorium maturation and successful infection. In a previous study performed in the laboratory of molecular applied microbiology at the Graduate School of Agriculture – Hokkaido University, an ortholog gene for p53BP1, a signal transducer protein that participates in G2-M cell cycle checkpoint in higher eukaryotes, was identified in the genome of *P. oryzae* and the phenotype of deletion mutants was characterized. Deletion mutants showed no significant deficiency in vegetative growth compared to wild-type and complemented strains, even on the media containing DNA damaging agents. However, these null mutants presented abnormalities in appressorium formation; the number of appressoria per conidium was higher than wild-type, leading to the incapacity of plant infection.

Although *Mop53BP1* is not crucial for a proper vegetative growth, the absence of this gene affected the appressorium development and infection process of *P. oryzae* mutants. Therefore, the main objective of this work is to clarify the importance of *Mop53BP1* during appressorium formation by means of gene expression analysis and studying the relationship of Mop53BP1 with proteins related to cell cycle progression.

CHAPTER TWO

Expression analysis of *Mop53BP1*

Chapter 2

2. Expression analysis of *Mop53BP1*

2.1. Expression analysis of Mop53BP1 in the presence of DNA damage agents

To test the response to DNA damage agents and for a better understanding of the physiological function of *Mop53BP1*, the expression of this gene was evaluated in wild-type strains cultured in liquid media supplemented with 4 different DNA damaging agents - MMS, Hydroxyurea (HU), Methyl viologen (MV) and heat shock (HS). In addition, the positive control *Rhm51* (ortholog of RAD51 in *Magnaporthe* described by Ndindeng et al. (2010)) was used for comparison purposes.

Material and Methods

2.1.1. DNA damage treatments for gene expression study

P. oryzae Ina 168 and Ina 86-137 were inoculated on oatmeal agar (OMA) plates and incubated at 25 ^{o}C. After 5 days the cultures were transferred to an incubator with fluorescent light and incubated for 3 days to produce enough conidia. After this period, 10 ml of 2YEG medium (0.2% yeast extract and 1% glucose) were added to the plates, and a loop used to scrap off the conidia. Conidia suspensions were inoculated into 100 mL of 2YEG medium at an inoculum level of 10^7 spores/mL and grown in Sakaguchi flasks using horizontal shaking at 27 °C for 3 days. After growth, each strain was submitted to 4 different treatments during 1 hour; MMS (Methyl methanesulfonate), an alkylating agent, was added to the culture until a final concentration of 0.2%. DNA synthesis inhibitor HU (Hydroxyurea) was added to a final concentration of 100 mM, to investigate the expression related to the cell cycle progression. In a third procedure MV (Methyl viologen) was added to a final concentration of 10 mM. This organic compound also known as Paraquat is a toxic component used in non-selective herbicides. Finally,

in the fourth treatment, the culture was submitted to a heat shock, elevating the temperature to 42 °C, then assessing the influence of temperature in *Mop53BP1* expression.

2.2.2. RNA extraction and qRT-PCR reaction

After treatments, mycelia were harvested by filtration, and RNAs were extracted using RNAiso Plus according to manufacturer's instructions (Takara, Shiga, Japan). The extracted RNAs were treated with DNase using an RQ1 RNase-Free DNase (Promega, Wisconsin, USA).

First, as a semi-quantitative, a reverse-transcription polymerase chain reaction (RT-PCR) was performed using the SuperScript® III One-Step RT-PCR (Life Technologies, Carlsbad, CA, USA) (see Appendix-I for PCR conditions). The primers used in the (RT-PCR) were Mop53BP1F and Mop53BP1R (Table 1).

Thus, for the quantitative real-time PCR assay (qRT-PCR), RNAs were used as templates for cDNA synthesis using the SuperScript® VILO™ cDNA Synthesis Kit (Life Technologies, Foster City, CA, USA). The 10-fold diluted reaction mixtures were applied to quantitative PCR analysis using the StepOnePlus™ Real-Time PCR Systems (Applied Biosystems, Foster City, CA, USA) with SYBR® Green PCR Master Mix (Life Technologies, Carlsbad, CA, USA). The primer pair 53BP1 qF and 53BP1 qR (Table 1) was used to amplify the p53BP1 gene. For the housekeeping gene, the primers actqF and actqR (Table 1) were used to amplify the Actin gene (MGG_03982.6). Also as a positive control, the expression of *Rhm51* (*RAD51* homolog) was evaluated (Ndindeng et al. 2010) (see Appendix-I for reactions conditions).

Results

A semi-quantitative test to confirm the RNA quality was performed by the RT PCR of *Mop53BP1* using the RNA extracted from the 4 different treatments. After confirmation of RNA quality (Fig. 8a) the expression of *Mop53BP1* and *Rhm51* was analyzed by quantitative real-time PCR assay (Fig. 8b). The expression of *Mop53BP1* was low for all treatments. However, the positive control *Rhm51* (ortholog of RAD51 in *Magnaporthe* described by Ndindeng et al. (2010)) showed elevated expression in treatments with MMS and MV (15 fold-increase in gene expression) and HU (4-5 fold-increase) (Fig. 8b).

Discussion

After *Mop53BP1* expression and localization analyzes during vegetative growth and appressorium development, it is possible to argue that *Mop53BP1* does not have a crucial role in the vegetative growth and DNA double-strand break repair in *P. oryzae*. Accordingly, the results obtained by (Tashika et al. unpublished data) showed that *Mop53BP1* deletion did not affect *P. oryzae* vegetative growth even in the presence of DNA damaging agents. Similar to these results, the deletion of ortholog *Hsr-9* from *C. elegans* did not affect post-embryonic development after γ-ray treatment, and *hsr-9* mutations did not prevent the cell cycle arrest induced by DSBs (Ryu et al. 2013).

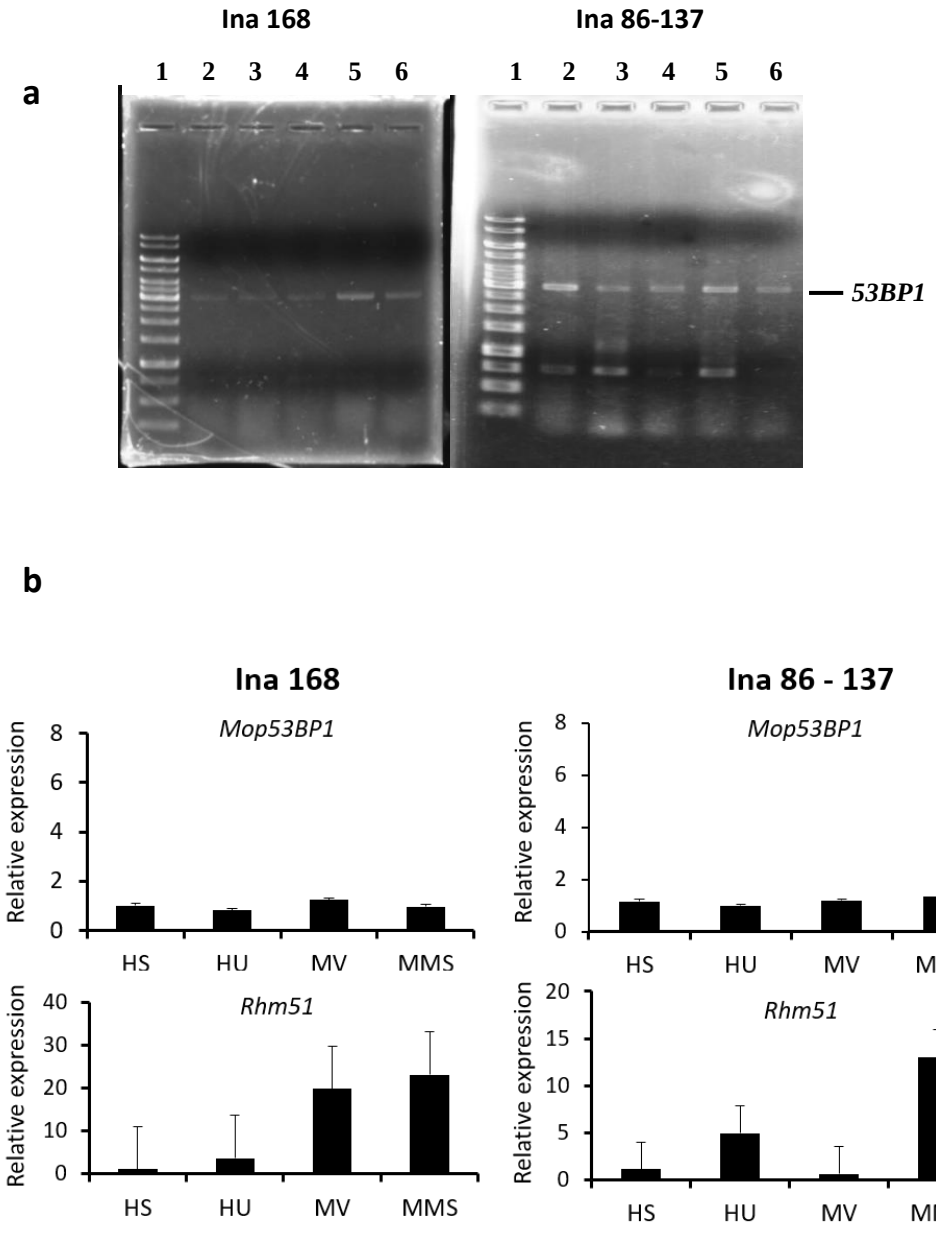

Figure 8. Expression analyzes of Mop53BP1 exposed to different DNA damage treatments. (a) RT-PCR for *Mop53BP1* amplification after DNA damage treatments. 1-1KB ladder, 2-Control, 3-HS, 4-HU, 5-MV, 6-MMS. (b) Real-time PCR results for *Mop53BP1* expression in the presence of DNA damage agents HU, MV, MMS, and heat shock, after grown on 2YEG medium for 3 days. The expression of *Rhm51* (*RAD51* homolog) was evaluated as a positive control.

2.2. Cellular localization and expression of Mop53BP1 in P. oryzae

To evaluate the role of Mop53BP1 during the appressorium differentiation, we produced $P_{Mop53BP1::}$eGFP::*Mop53BP1* by fusing eGFP to the N-terminus of *Mop53BP1*, and conducted a microscopic observation of different stages of appressorium development (conidia, germ tube, and appressorium). This strategy was also suitable to verify the cellular localization of *Mop53BP1*during appressorium formation. A qRT-PCR was performed in order to analyze the gene expression during the first hours of appressorium development.

Material and Methods

2.2.1. Construction of pBLASTR-DEST-$P_{Mop53BP1}$::eGFP::*Mop53BP1* plasmid

To construct the pBLASTR-DEST-$P_{Mop53BP1}$::eGFP::*Mop53BP1* plasmid, a 4.0-kb genomic DNA fragment containing the native promoter of Mop53BP1 was amplified using the KOD FX polymerase (Toyobo, Osaka, Japan) and primers Promoter-Mop53BP1F and Mop53BP1R (Table 1) (*Mop53BP1* sequence was checked by sequence reaction) (see Appendix-I for PCR conditions). The amplified fragment was inserted into the pENTR/D-TOPO vector to produce pENTR-$P_{Mop53BP1}$*Mop53BP1*. This vector was subsequently used as a template for inverse PCR reaction (primers Inv2F and Inv2R (table 1) - KOD FX polymerase, see Appendix-I for PCR conditions), to construct pENTR-$P_{Mop53BP1::}$eGFP::*Mop53BP1* using the T4 DNA ligase (see Appendix-I for ligation conditions). The eGFP fragment was amplified from the pPCG664 plasmid (provided by Dr. T. Kamakura, Tokyo University of Science) using the primers eGFP-F and eGFP-R (Table 1) and tagged at N-terminus (see Appendix-I for PCR conditions). The pENTR-$P_{Mop53BP1::}$eGFP::*Mop53BP1* was then transferred to the blasticidin S-resistant pBLASTR-DEST-$P_{Mop53BP1::}$eGFP::*Mop53BP1* via an LR reaction using Gateway LR

Clonase II Enzyme mix (Invitrogen, Life Technologies Japan Ltd., Tokyo, Japan) (see Appendix-I for reaction conditions) (Fig. 9).

2.2.2. Fungal transformation

Spore suspensions (10^5) of INA86-137 *Mop53BP1* disruption mutants were inoculated into 200 mL of 2YEG in Erlenmeyer flasks and incubated at 25 °C for 3 days. After this period, around 2 grams of growth mycelia were separated from the media by filtration using a miracloth-1R (CALBIOCHEM, EMD, Germany) and digested by adding 10 mL of digestion buffer (see Appendix-I for composition) and incubating at 37 °C for 1 h with shaking at 20 rpm. After digestion, the protoplasts were collected by filtration using a new miracloth-1R and the filtrate was centrifuged at 3500 x g for 10 minutes at 4 °C. The supernatant was discarded and the protoplast were washed with 500 µL of STC solution (see Appendix-I for composition) and centrifuged as above. Finally, the protoplasts were resuspended in 300 µL of STC and their concentration was checked by counting using a Neubauer hemocytometer.

The protoplast concentration was adjusted to 10^7 cells/mL, and 10 µg of the linearized plasmid pBLASTR-DEST-P$_{Mop53BP1}$::eGFP::*Mop53BP1* were added to 100 µL of protoplast solution in a 50 mL falcon tube and incubated on ice for 20 min. After that, 2 mL of polyethylene glycol (PEG) solution (see Appendix-I for composition) was added to the sample and incubated on ice for 20 min. The total solution was supplemented with 30 mL of STC and centrifuged at 3500 x g for 15 min. The supernatant was removed and the protoplasts were resuspended with 200 µL of STC solution. Finally, samples were mixed with 25 mL of bottom-agar media (see Appendix-I for composition) and poured into plates, allowed to solidify and incubated at 27 °C for 24 hours.

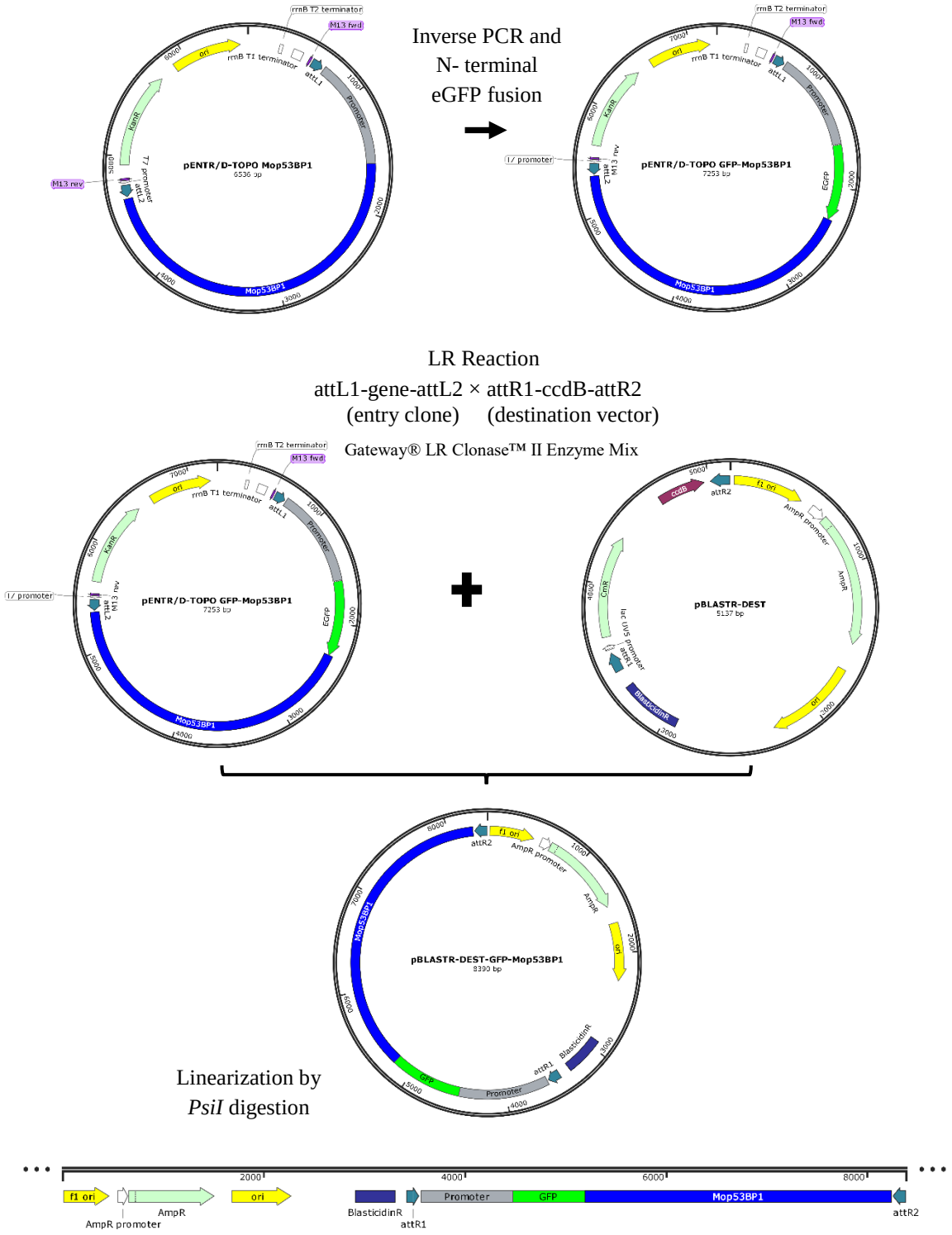

Figure 9. Construction of pBLASTR-DEST-P*Mop*53BP1::eGFP::*Mop53BP1* plasmid.

After inverse PCR and LR-clonase reaction steps, the destination vector was linearized with *PsiI* and used to transform INA86-137 *Mop53BP1* disruption mutants.

After protoplast regeneration during 24 h, top-agar (see Appendix-I for composition) containing 5 µg/mL blasticidin was poured on the plates, which were incubated at 27 °C for 6 days. Colonies that were capable of growing into the top-agar were considered mutants and then transferred onto 2 mL of OMA in microwell plates supplemented with 5 µg/mL blasticidin. These plates were incubated at 27 °C for 6 days, and after this period, a slant of each colony in the well was collected and spread on water agar (4% agar) by gently dragging the slant on the medium. The water agar plates were incubated for 24 h at 27 °C, and after that, a single conidia isolation was performed by picking up germinating conidia visualized by microscope. Those single conidia were transferred on prune agar (see Appendix-I for composition) containing 5 µg/mL blasticidin and incubated at 27 °C for 6 days.

2.2.3. Screening of mutants by PCR and Southern Hybridization

Transformants that grew on prune agar were inoculated into 40 mL of 2YEG supplemented with 5 µg/mL blasticidin in a 100 mL Erlenmeyer flask and incubated at 27 °C for 6 days on a horizontal shaker at 100 rpm. After this period, the mycelia were filtered, freeze dried overnight and subsequently powdered by using a cell disruption centrifuge. After that, the disrupted cells were resuspended in 500 µL of DNA extraction buffer (see Appendix-I for composition) by vortexing. The DNA was then extracted using the phenol/chloroform method and precipitated with isopropanol. The samples were preserved in TE buffer and stored at -20 °C. The DNA concentration was checked in the next day.

The genomic DNA extracted from the transformants were used as a template for the PCR performed with the KOD FX polymerase and primers eGFPF and Mop53BP1R (Table 1) (see Appendix-I for PCR conditions).

The southern hybridization was performed using 3 µg of genomic DNA from transformants, which were digested with Hind III HF® and EcoRI HF® restriction enzymes (New England Biolabs, Ipswich-Massachusetts, United States) (see Appendix-I for digestion conditions). Those enzymes targeted the two flanking regions of Promoter-Mop53BP1 in *P. oryzae* genome. After digestion, the samples were ethanol-precipitated and separated on a 1% Seakam-GTG agarose gel, stained with ethidium bromide, and photographed by UV detection. The gel was then soaked in depurination solution (see Appendix-I for composition), denaturation solution (see Appendix-I for composition) and in a neutralization solution (see Appendix-I for composition) for 30 min each solution. Blotting was performed according to Sambrook and Russel (2001) using a Hybond-N^+ nylon membrane attached to the gel and soaked in 20 x SSC (see Appendix-I for composition) as the transfer solvent. After overnight blotting, the membrane was removed, soaked in 6 x SSC for 5 minutes and the present DNA was submitted to cross-link using a UV spectrolinker (Spectronics Corp., Japan) applying 1200 x 100 µJ/cm^2. The amplified eGFP fragment was used as a probe, and the gene images Alkphos Direct Labelling and Detection System (GE Healthcare) procedures were used to label the eGFP fragment, hybridization, post-hybridization stringency washes, signal generation and detection. The bands on the membrane were visualized with imagequant LAS 4000 (Fujifilm Life Science, Roche Diagnostics), after 4 h of exposure.

2.2.4. Appressorium induction and evaluation of *Mop53BP1* expression during appressorium formation

P. oryzae confirmed mutants (complementation mutants with Mop53BP1-tagged GFP) were grown on OMA plates and incubated at 25 ºC. After 5 days, the cultures were transferred to an incubator with fluorescent light and incubated for 3 days in order to

produce enough conidia. These conidia were flushed with 5 mL of sterile distilled water (SDW) filtered with a miracloth-1R and counted using a hemocytometer. Thus, 10^5 cells/mL of conida suspension were pipetted as drops of 2 µL on hydrophobic microscope glass slides. These glass slides were incubated at different times in order to monitor the GFP fluorescence during appressorium formation. For nuclei visualization samples were soaked in 10 µg/ml DAPI (2,4, -Diamidino-phenyl-indole) solutions in the dark for 5 min before epifluorescence microscopy examination. All the microscopic analyses were conducted using a BX-50 fluorescent microscope (Olympus, Tokyo, Japan) that was equipped with a U-MNIBA3 filter set.

In addition, to complement the analyzes of *Mop53BP1* expression during appressorium formation, a Real-Time PCR was conducted evaluating the 9 first hours of appressorium development. Thus, for RNA extraction, conidia (~ 1×10^5 /ml) were collected from hydrophobic microscope glass slides which were incubated at 27 °C at different times. The RNeasy® Mini Kit (Qiagen) for extraction and purification was used because of small amounts of starting cell material. Then, DNAse treatment, RT-PCR, and qRT-PCR were performed as described in section 2.2.2.

Results

After PCR and Southern Hybridization confirmation (Fig. 10a), the cellular localization of Mop53BP1 was assessed on conidia, germ tube and appressorium formation of *Mop53BP1-GFP2* and *Mop53BP1-GFP 4* complementation mutants. All mutants presented the same fluorescence pattern. Initially, fluorescent signals were mainly observed in the nuclei regions of conidia cells. Suggesting that Mop53BP1 colocalize with nuclei during the first hours of appressorium formation (Fig. 10b).

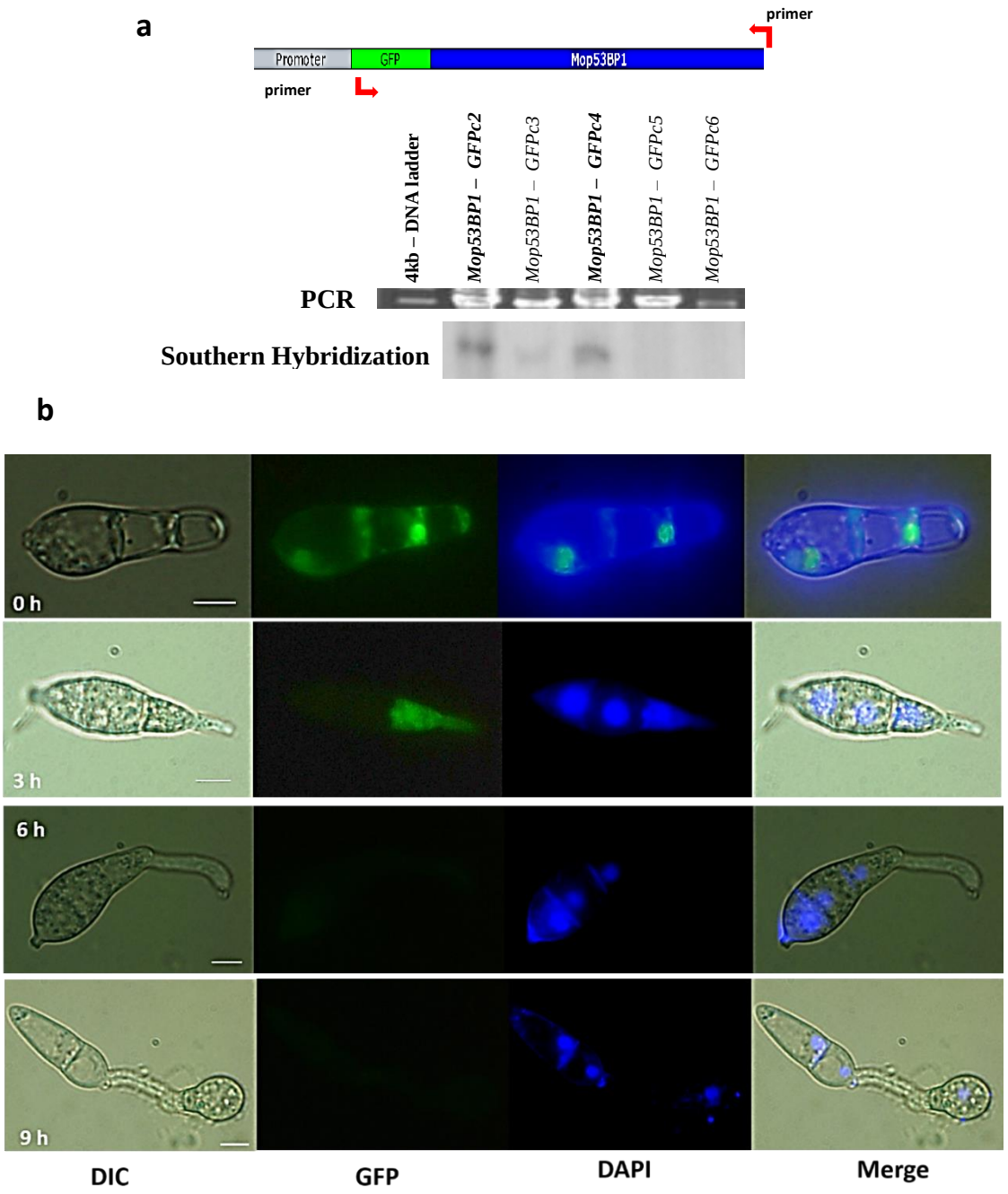

Figure 10. Confirmation of positive transformants and expression of the GFP-Mop53BP1 construct. (a) PCR performed with primers eGFPF and Mop53BP1R (Table 1), and Southern hybridization by digesting genomic DNA with Hind III and EcoRI and using eGFP fragment as a probe. (b) Expression of the GFP-Mop53BP1 fusion under the control of the native promoter during appressorium formation. Scale bar = 5 µm.

After 3 hours, in the initial stage of germ tube, the fluorescence was observed only in the conidia cell that would develop the appressorium. Subsequently, the fluorescence signals in the completed germ tube and appressorium structures turn to be undetectable (Fig. 10b).

In addition, RT PCR and qRT-PCR analyzes of 9 first hours of appressorium formation revealed that *Mop53BP1* expression was highest at the initial point and decreased according to appressorium development (Fig. 11a and 11b). These results suggest that *Mop53BP1* expression occurs during the first hour of appressorium formation.

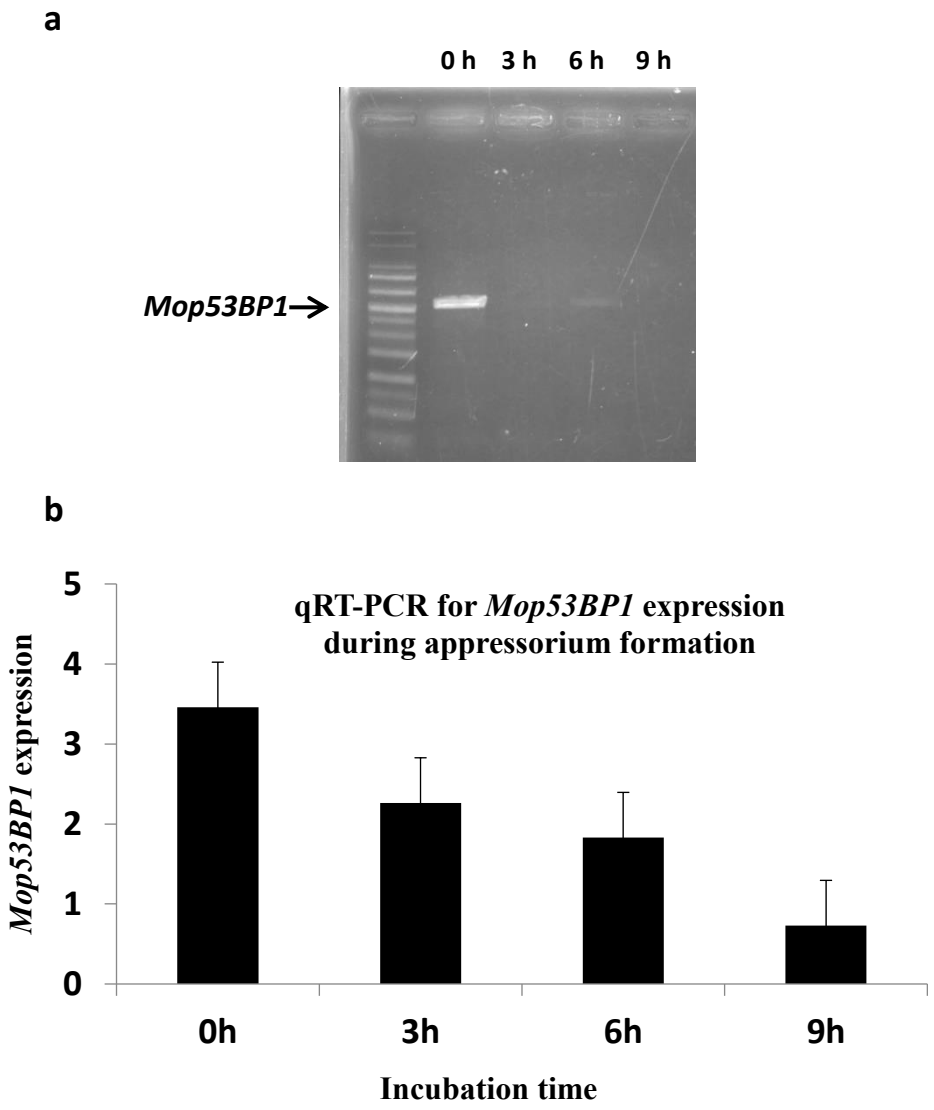

Figure 11. Expression analyzes of Mop53BP1 during the first hours of appressorium formation (a) RT-PC and (b) qRT-PC for *Mop53BP1* expression during 0h, 3h, 6h and 9h of appressorium development.

Discussion

Despite previous results about *Mop53BP1* expression during vegetative growth, the analyses of nucleus dynamics, protein localization, and expression timing during appressorium formation revealed that this gene has an important role in the development of a proper appressorium structure. According to our results, the expression of *Mop53BP1* occurs during the first hours of appressorium formation, and this protein co-localizes to conidial nuclei. The same protein localization was found (Ryu et al. 2013; Jakob et al. 2009; Du et al. 2003) when p53BP1 and orthologs were tagged to fluorescent markers. After that Mop53BP1 is present in the conidial cell that would generate the appressorium structure, which is an interesting feature since the mitosis process and the G2/M checkpoint are taking place in this cell (Saunders et al. 2010).

Eventually, *Mop53BP1* null mutants displayed multiple appressoria structures per conidia, and the collapse of the spore followed by nuclear degeneration did not occur (Tashika et al. unpublished data). This autophagy process is crucial to regulating the turgor of appressoria, since it is involved in the degradation of lipid storage reserves and act as a source of osmotically active metabolites that generate the very high turgor pressures enabling the penetration of fungal pathogens into host plant tissues (Liu et al. 2015). Another important feature is that autophagic cell death of the fungal spore is also coupled to mitotic completion, which is completed before the morphogenesis of the appressorium, suggesting that either a G2/M or a postmitotic checkpoint may regulate appressorium formation in *M. oryzae* (Veneault-Fourrey et al. 2006)

We first inferred that Mop53BP1 is expressed in the first hours of appressorium formation and is might working during cell cycle checkpoints G1/G2/M. A potential hypothesis is that Mop53BP1 is interacting with Serine/threonine-protein kinase Chk1, similar to Crb2 from *S. pombe* (Saka et al. 1997). Chk1 is responsible for mediating the

inhibitory phosphorylation of B-type cyclin–CDK1, and consequently, arrest the cell cycle during DNA damage or in the presence of unreplicated chromatin (Osés-Ruiz et al. 2016).

A possible interaction of Mop53BP1 and cyclin-dependent kinase could explain the multiple abnormal appressoria developed by *ΔMop53BP1* mutants, since the appressorium formation is a precise and timing dependent cell cycle progression, and a delay caused by deletions or modifications of genes that participate in this process can directly affect the infection success.

Table 1. Synthetic oligonucleotides used in the expression analysis and localization of Mop53BP1.

Primer name	Sequence (5'-3')	Target gene	Application
Mop53BP1F	ATGGCTAAGAAGAAGG CAAAACCAA	*Mop53BP1* ORF	RT-PCR for *Mop53BP1* transcript
Mop53BP1R	TCACTCCTCCATCTCCTC TGGTTCT	*Mop53BP1* ORF	RT-PCR for *Mop53BP1* transcript
53BP1qF	TTTGCCATCTCCTTTTCA TCAA	*Mop53BP1* ORF	qRT-PCR for *Mop53BP1* transcript
53BP1qR	CGGTGAGGCCACTGTAT TCA	*Mop53BP1* ORF	qRT-PCR for *Mop53BP1* transcript
actqF	CTGCCCAGAGCTCCAGC TT	*P. oryzae actin ORF*	qRT-PCR for actin transcript
actqR	CGTTGCCGATGGTGATA ACC	*P. oryzae actin ORF*	qRT-PCR for actin transcript
eGFPF	ATGGTGAGCAAGGGCG AGGA	eGFP	eGFP amplification
eGFPR	TTACTTGTACAGCTCGT CCATGCCG	eGFP	eGFP amplification
Inv2F	ATGGCTAAGAAGAAGG CAAAACCAAAGC	End of *Mop53BP1* promoter	Inverse PCR for eGFP insertion
Inv2R	CGTCTGAGAGATTGCTG CCGTTTTC	ORF start of *Mop53BP1*	Inverse PCR for eGFP insertion

CHAPTER THREE

Overexpression of *Mop53BP1* and interaction with other proteins

Chapter 3

3. Overexpression of *Mop53BP1* and interaction with other proteins.

3.1. Construction of overexpression mutants

To evaluate whether the level of Mop53BP1 expression is important for pathogenicity or not, as well as to confirm the exact localization of this protein during all steps of appressorium development, we replaced the native promoter by the constitutive TEF1 gene promoter region. Therefore, we produced a *Mop53BP1* overexpression mutant, and performed several assays comparing vegetative growth and appressorium formation of wild-type, Mop53BP1 deletion and overexpression mutants.

Material and Methods

3.1.1 Construction of pBLASTR-DEST-TEF::eGFP::Mop53BP1 plasmid and transformation

To study the influence of *Mop53BP1*overexpression, we replaced the native promoter by the constitutive TEF1 gene promoter region. TEF gene codes for the translation elongation factor 1α. This protein is responsible for the translocation of amino acyl tRNAs to the ribosome and is one of the most abundant soluble proteins in eukaryotic cells. Elongation factors are responsible for achieving an accuracy of translation and are remarkably conserved throughout evolution (Steiner and Philippsen, 1993). Therefore, the vector pENTR-P$_{Mop53BP1::}$eGFP::*Mop53BP1* (from section 2.2.1) was opened by inverse PCR using the primers Invfwr and Invrev (Table 2). TEF1 promoter region was amplified from *P. oryze* genomic DNA using the primers TEFf and TEFr (Table 2). Subsequently, the reaction product was purified and used as a template for a new amplification using the overlapping pair of primers TEFovf and TEFovr (Table 2) (TEF

promoter sequence was checked by sequence reaction). The products of inverse and overlapping PCR were fused using NEBuilder® HiFi DNA Assembly kit.

The pENTR-TEF1::eGFP::*Mop53BP1* was then transferred to the blasticidin S-resistant pBLASTR-TEF1::eGFP::*Mop53BP1* via LR reaction using Gateway LR Clonase II Enzyme mix (Invitrogen, Life Technologies Japan Ltd., Tokyo, Japan) (Fig. 12). Similar to section 2.2.1 and 2.2.2, the pBLASTR-TEF::eGFP::*Mop53BP1* plasmid was linearized using *PsiI* restriction enzyme and transformed into INA86-137 wild-type and *Mop53BP1* disruption mutant. The verification of positive transformants was performed according to section 2.2.3 (the conditions of all PCR reactions are listed in Appendix-I).

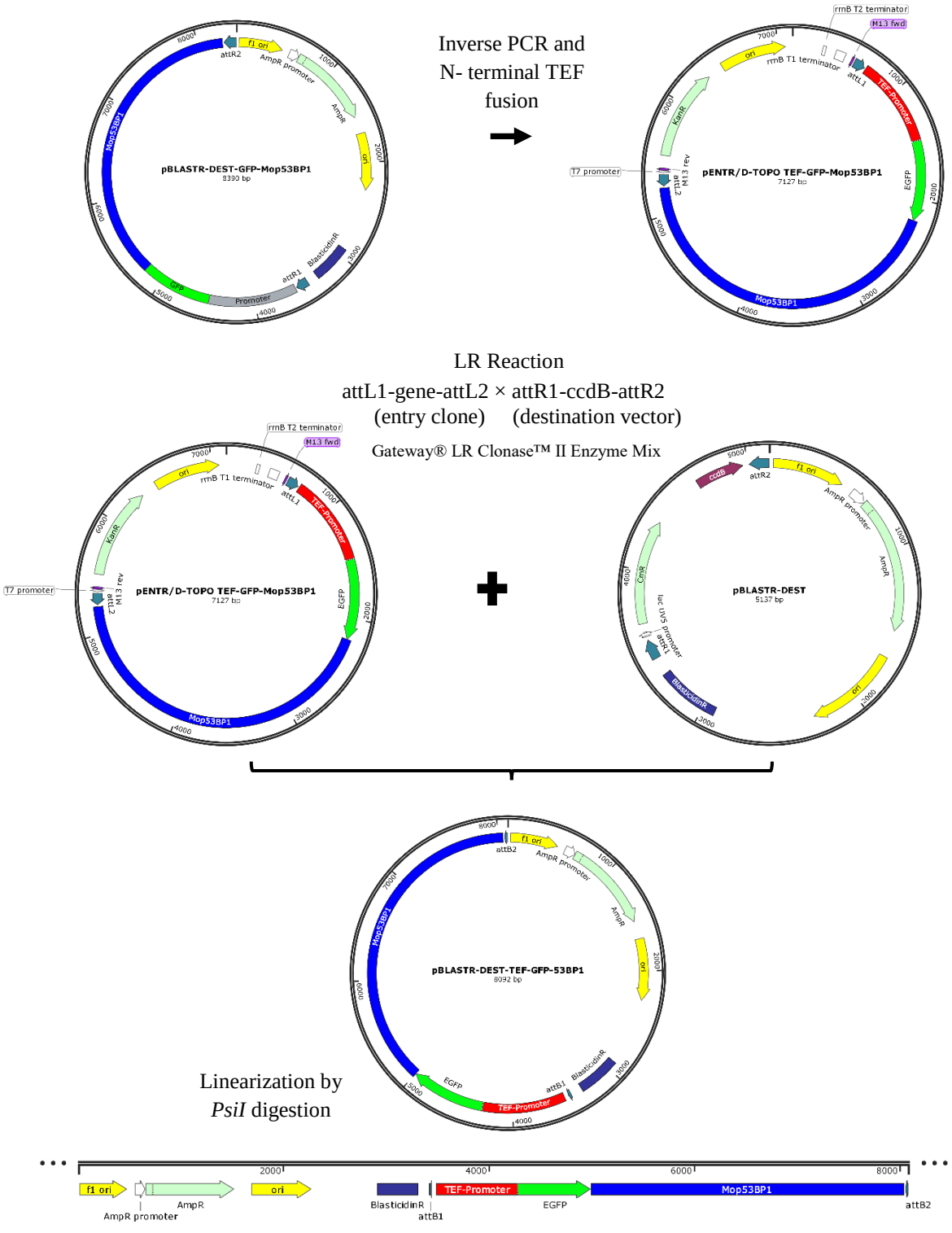

Figure 12. Construction of pBLASTR-DEST-TEF::eGFP::*Mop53BP1* plasmid.

The destination vector was linearized with *PsiI* and used to transform INA86-137 *Mop53BP1* wild-type and disruption mutants.

3.1.2. Appressorium induction using onion epidermis membrane and evaluation of *Mop53BP1* overexpression

Firstly, conidia suspensions of *P. oryzae* confirmed mutants were inoculated on hydrophobic microscope glass slides, after that, DAPI and GFP fluorescence observations during appressorium development were performed according to section 2.2.4.

The spore suspensions were also inoculated on onion epidermis membrane. This assay is a rapid way to evaluate the proper appressorium formation and pathogenicity of *P. oryzae* mutants. Therefore, onion cells were prepared by separating the layers of fresh onion. The membrane was obtained by peeling a single layer using sterilized tweezers. After that, those membranes were soaked into SDW and heated in the microwave for 40 s to neutralize the sulfur compounds and reduce the acidity of onion. Finally, the membranes were placed on glass slides and inoculated with diluted conidial suspensions from transformants (10^4~10^5 cells/mL) by dropping about 10 drops (1 µL/drop) of suspension and incubating at 27 °C. Fluorescence visualization was then performed at different times as a time course assay.

3.1.3. Comparisons between vegetative growth of wild-type, *Mop53BP1* deletion, and overexpression mutants.

In order to verify the effect of *Mop53BP1* overexpression in *P. oryzae* vegetative growth, conidia suspensions from wild-type, *Mop53BP1* deletion (constructed by (Tashika et al. unpublished data)) and overexpression strains were inoculated into 40 mL of 2YEG (2 g yeast extract, 10 g glucose per liter) medium at an inoculum level of 10^7 spores/mL, and grown in Erlenmeyer flasks using horizontal shaking at 27 °C for 24 hours. Thus, aliquots of 100 µL were added on glass slides in different stages of vegetative

growth, and conidia development was accessed by microscope observations as a time course assay.

Results

After PCR and Southern Hybridization confirmation (Fig. 13), the cellular localization of Mop53BP1 overexpression was assessed on conidia, germ tube and appressorium formation of *Mop53BP1-TEF1*, *Mop53BP1-TEF2* (resulting from the transformation using WT strain), *Mop53BP1-TEFC2* and *Mop53BP1-TEFC3* (resulting from the transformation using *ΔMop53BP1* strain) mutants.

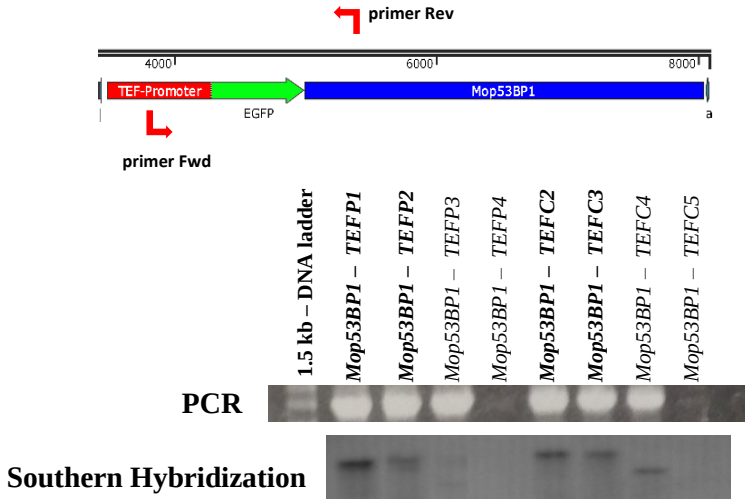

Figure 13. Confirmation of positive transformants. PCR performed with primers TEF-GFPfw and 53BP12R (Table 2), and Southern hybridization by digesting genomic DNA with KpnI and EcoRI and using eGFP fragment as a probe.

The confirmed mutants presented the same fluorescence pattern; a strong green fluorescence was observed on all the stages of appressorium formation, mainly in the

nuclei regions of cells (Fig. 14). Also, when *Mop53BP1*overexpression mutants were inoculated on onion epidermis surface, normal appressorium and infection were observed (Fig.15). The fluorescence pattern was similar to that observed in initial conidia during appressoria development on glass slide, strong, round shape and usually localized to the nuclei. Moreover, after invasive hyphae formation, fluorescence signals have still been detected (Fig. 15). These results suggest that overexpression of Mop53BP1 will not affect the appressorium formation and infection, and that the protein localizes to nuclei during all steps of plant infection. Also, according to Fig. 16, wild-type, *ΔMop53BP1* and overexpression mutants showed no significant difference in vegetative growth on 2YEG liquid medium.

Discussion

The overexpression mutants confirmed the localization of Mop53BP1 accordingly to the previous chapter and to the reports of Ryu et al. (2013), Jakob et al. (2009) Du et al. (2003) when p53BP1 and orthologs were tagged to fluorescent markers. In addition, the mutants obtained from the complementation of *ΔMop53BP1* could develop normal appressorium and infection, showing that the overexpression did not affect the pathogenicity of *P. oryzae*. Thus, the analyses of nuclear dynamics, protein localization and expression time course during appressorium formation (chapters 2 and 3) revealed that this gene has a unique role in the control of appressorium formation.

During the interaction between *P. oryzae* and the host, some receptors and sensors recognize the host surface and activate signal transduction pathways for appressorium development and infection. This process initiates by chemical and physical recognition, the receptor PTH1 in the plasma membrane is responsible for sensing the hydrophobic surface, while receptors as Msb2 and Sho1 recognize the plant epicuticular wax (Li et al.

2012). Consequently, these sensor proteins (coupled to G-proteins as Mgb1, MagA and MagB) activate two major pathways; cyclic AMP-protein Kinase A (cAMP-PKA) and Pmk1 mitogen-activate protein kinase (MAPK). These pathways are responsible for appressorium formation and maturation, nuclear degradation/autophagy, invasive growth and disease development (Wilson and Talbot 2009).

Due to the fact that appressorium development is a timely and precise cell cycle dependent process, the subsequent assays will focus on elucidating the role of Mop53BP1 during all stages of conidia cell division until the completion of appressorium structure.

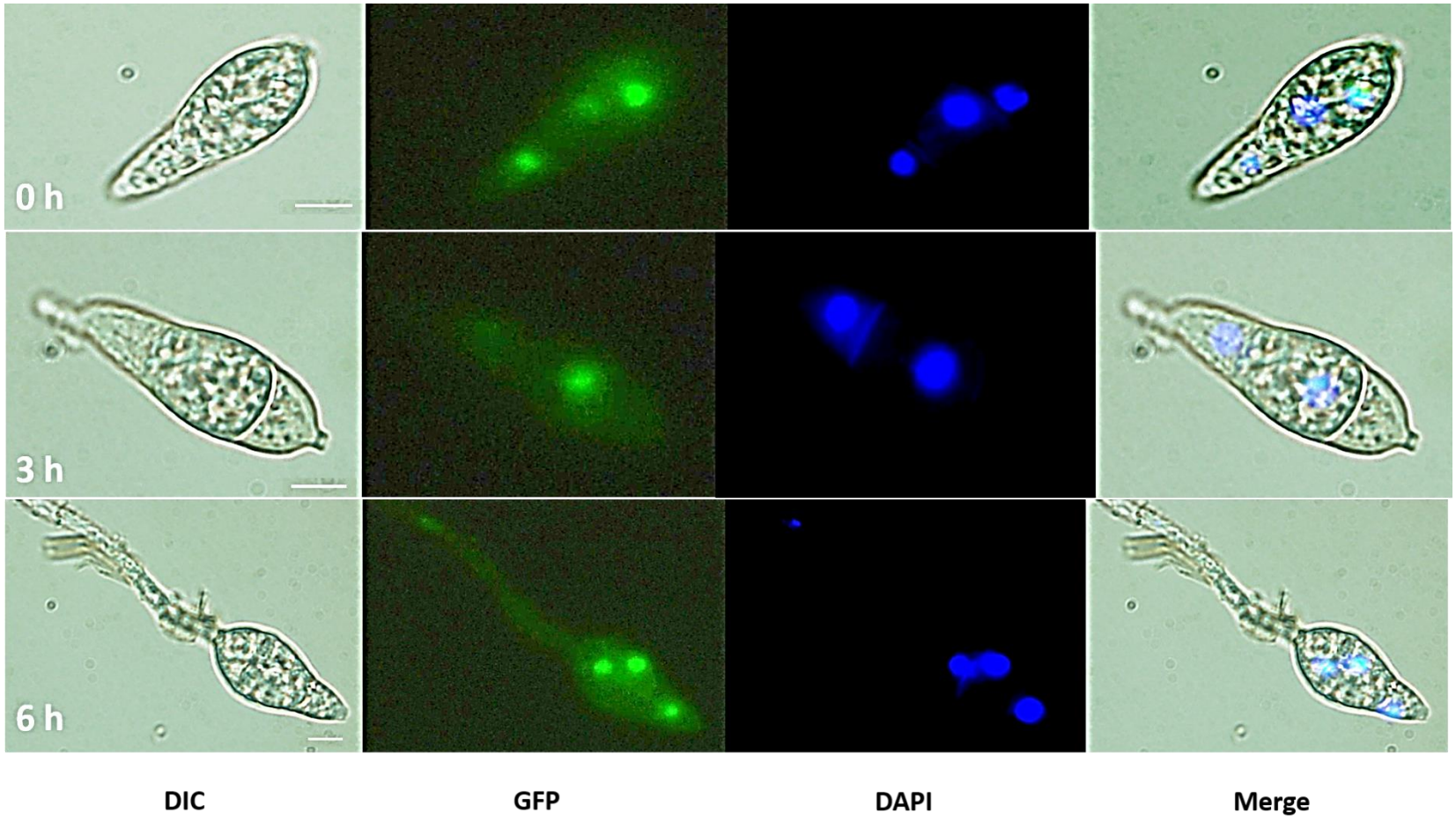

Figure 14. Expression of the GFP-Mop53BP1 fusion under the control of TEF1 promoter during appressorium formation. Strong green fluorescence was observed in the nuclei regions of cells on glass slides surface. Scale bar = 5 μm.

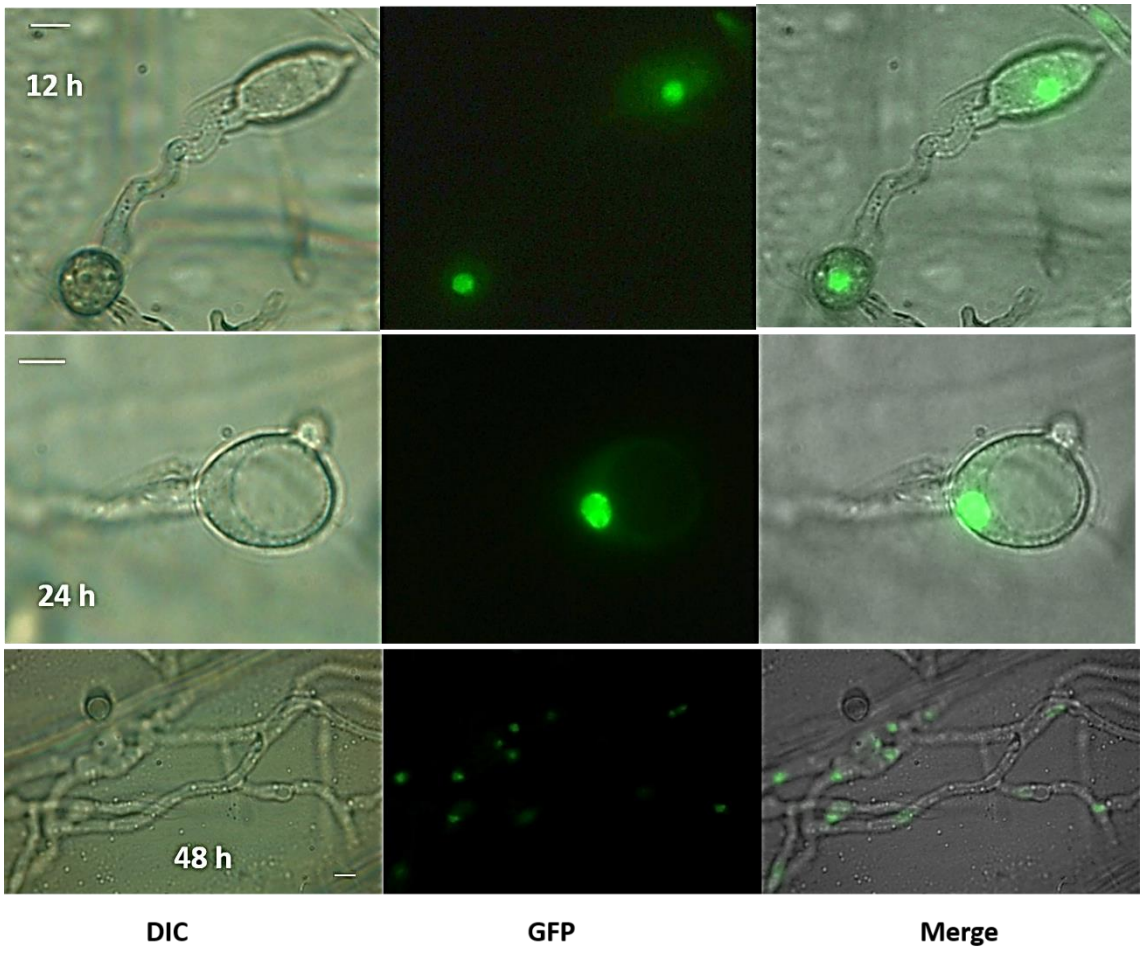

Figure 15. Expression of the GFP-Mop53BP1 fusion under the control of TEF1 promoter during appressorium formation and onion epidermis infection. Fluoresce exhibit the same pattern during all steps of plant infection and signals were also detected after invasive hyphae formation. Scale bar = 5 μm

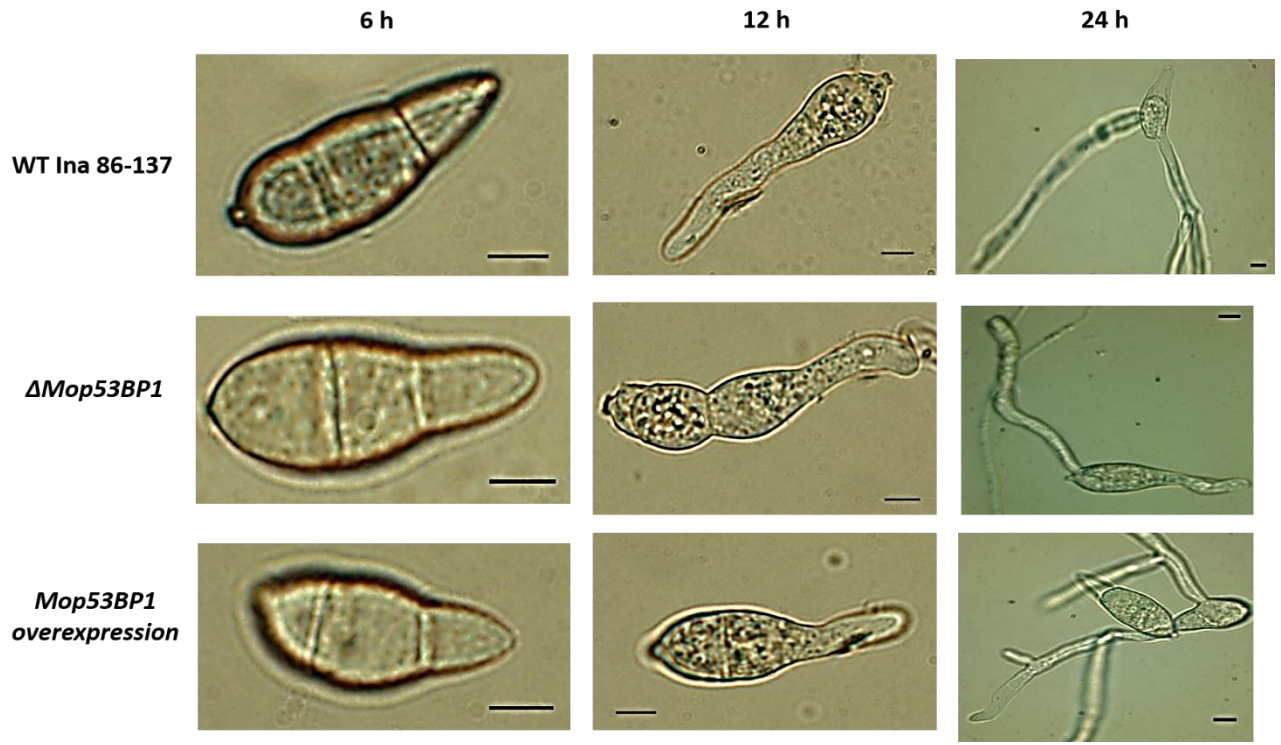

Figure 16. Comparison between vegetative growth of wild-type, *ΔMop53BP1* and overexpression mutants in 2YEG medium during 24 hours. No significant difference between strains growth was observed. Scale bar = 5 μm.

3.2. Interaction of Mop53BP1 with proteins related to cell cycle progression

As previous results suggested, Mop53BP1 may have some role related to DNA structure, function, and regulation processes during the cell cycle progression of appressorium formation. Our first hypothesis was that Mop53BP1 could work with proteins as cyclins, cyclin-dependent kinases or checkpoint kinases, recruited on the checkpoint for DNA replication completion. In order to investigate that, we monitored the growth of wild-type, Mop53BP1 deletion, and overexpression mutants in the presence of DNA synthesis inhibitor HU and microtubule inhibitor benomyl (Fig. 17).

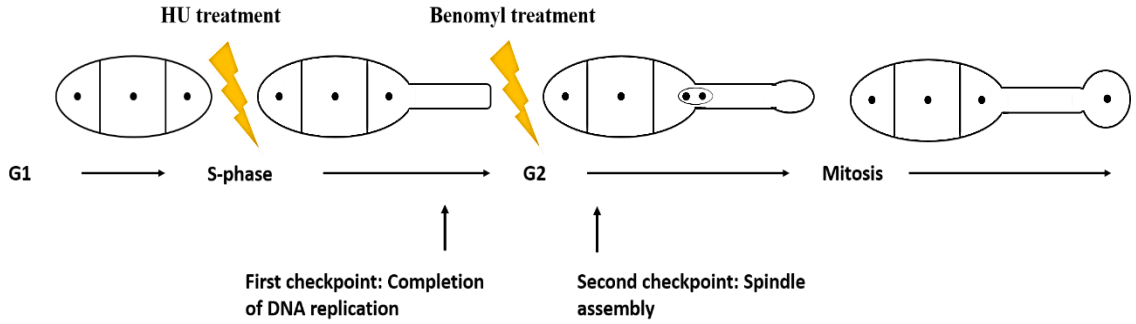

Figure 17. Scheme showing cell-cycle transitions necessary for appressorium-mediated plant infection by *M. oryzae*, indicating the target region for HU and Benomyl action.

Material and Methods

3.2.1. Monitoring the influence of Mop53BP1 in the cell cycle progression by using an inhibitor of DNA synthesis HU and the microtubule inhibitor benomyl.

To observe the effect of DNA replication inhibition, conidia suspensions of wild-type and *ΔMop53BP1* mutant were prepared by adding HU to a final concentration of 200 mM, then incubated on hydrophobic microscope glass slides at 27°C and observed after 24 h (similar to section 2.2.4). To show the effect of a G2 arrest, the same procedure was

performed using new spore suspensions and adding the microtubule inhibitor benomyl to a final concentration of 5 mg/mL^{-1}.

Results

Previous results suggested that Mop53BP1 may have some role related to the regulatory processes of appressorium formation which is participated in the nuclei. In order to clarify whether Mop53BP1 is related to the G1/S checkpoint or not, the appressorium formation of Mop53BP1 deletion mutant in the presence of DNA synthesis inhibitor HU was monitored. In the absence of HU, WT strain formed normal appressorium at 12 h, as expected. However, in the presence of HU, both WT and *ΔMop53BP1* were unable to develop appressoria (Fig. 18a) suggesting that, when DNA replication is inhibited, the cell cycle is arrested regardless of the presence of Mop53BP1. Therefore, Mop53BP1 may not have a role or interact with proteins responsible for DNA replication checkpoint.

In addition, to investigate whether the cell-cycle control at the G2/M boundary was disturbed by the absence of Mop53BP1 or not, we treated a WT strain and *ΔMop53BP1* mutant with the microtubule inhibitor benomyl. In the presence of benomyl, WT strain developed abnormal appressorium structures, as expected the appressorium failed to mature due to a disturbance on mitosis process, but deletion mutants could not develop germ tube, remaining at conidium stage (Fig. 18b).

Discussion

Mop53BP1 null mutants displayed hypersensitivity to benomyl, while overexpression mutants showed some resistance to the microtubule inhibitor. Several cases of resistance to benomyl and other benzimidazole fungicides have been reported (e.g. Yang et al. 2015; Liu et al. 2014; Fan et al. 2014; Zhang et al. 2010; Chung et al.

2010) in most cases, the resistance is associated with point mutations in β-tubulin gene which result in altered amino acid sequences at the benzimidazole binding site. This evidence contributes to another hypothesis that Mop53BP1 may interact with microtubule proteins as α, β, and γ tubulins during appressorium formation. Moreover, studies from Hsu et al. (2001) and Starita et al. (2004) about the breast and ovarian susceptibility gene BRCA1, reported a γ-tubulin-binding domain in BRCA1, and when this interaction was disturbed, abnormal spindle formation followed by abnormal mitotic cells were observed.

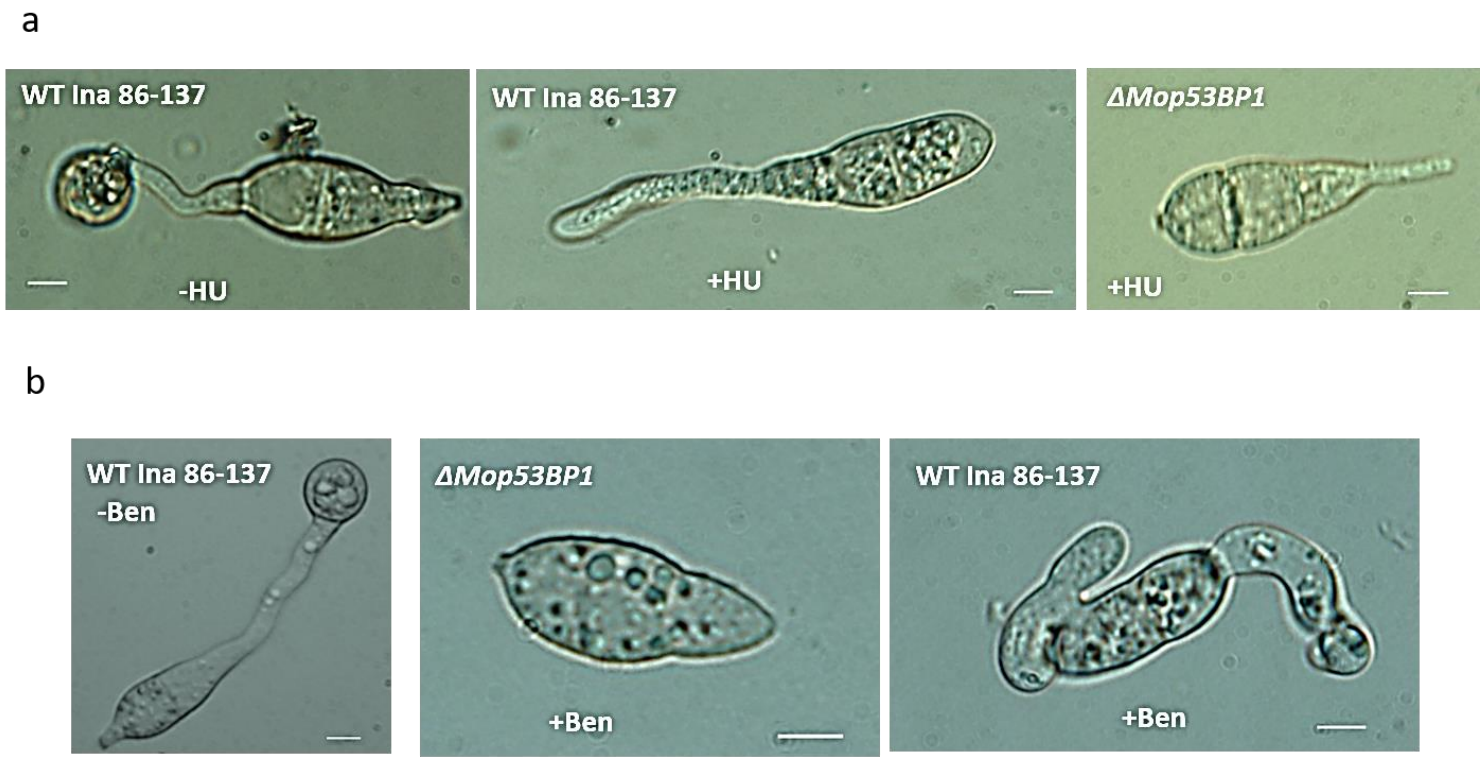

Figure 18. Appressoria development under exposure to HU and benomyl. (a) Appressorium formation by WT (control observed after 12 h) and *ΔMop53BP1* mutant following exposure to 200 mM HU, observed at 24 h. (b) Appressorium formation by WT (control observed after 12 h), *ΔMop53BP1*mutant and WT following exposure to benomyl (5 mg/mL^{-1}), observed at 24 h. Scale bar = 5 μm.

3.3. Evaluating the relationship between Mop53BP1 and the microtubule inhibitor benomyl

The previous assays involving the cell cycle progression and chemical inhibitors showed a hypersensitivity of *Mop53BP1* deletion mutants to the microtubule inhibitor benomyl. Therefore, we decided to analyze further the appressorium formation of deletion mutants exposed to different concentrations of benomyl. We also monitored the appressorium formation and pathogenicity of overexpression mutants exposed to benomyl.

Material and Methods

3.3.1. *Mop53BP1* deletion and overexpression mutants exposed to benomyl

Firstly, for a better comprehension of the hypersensitivity of *Mop53BP1* deletion mutants to the microtubule inhibitor benomyl, conidia suspensions of wild-type and deletion mutant ($10^4 \sim 10^5$ cells/mL) were prepared by adding the reagent in different concentrations; 5 mg/mL, 0.5 mg/mL, and 0.05 mg/mL. After that, the suspensions were inoculated on onion membranes, and the appressorium development was observed during different times.

The appressorium formation of overexpression mutants under exposure to benomyl was also evaluated. For that, conidia suspensions ($10^4 \sim 10^5$ cells/mL) were prepared by adding the microtubule inhibitor to a final concentration of 5 mg/mL. The suspensions were then inoculated on onion membranes as shown in section 3.1.2, and the appressorium development was observed during different time points.

Results

When exposed to different concentrations of benomyl, the deletion mutant and wild-type strain presented hypersensitivity, which increased proportionally to the amount of chemical used. However, the wild-type was able to form germ tube in all tested concentrations, and also developed normal appressoria in the lowest benomyl concentration (0.05 mg/mL). Different from the wild-type, *ΔMop53BP1*mutant could germinate the conidia only in the assay with the lowest concentration. Also, the abnormal appressoria structure reported by (Tashika et al. unpublished data) was coupled with irregular shape caused by benomyl treatment (Fig. 19).

The overexpression mutant was capable of forming appressorium (Fig. 20), while WT presented the same phenotype as described previously (Fig. 21). Interestingly, the appressorium of overexpression mutant could not penetrate into onion epidermis, indicating that the appressorium is not matured; on the other hand, the conidia cell in the opposite side of appressorium started to form germ tube. These results indicate that overexpression strain shows some resistance to the microtubule inhibitor benomyl and Mop53BP1 may have some role related to the function of microtubules.

These results suggest a possible relationship between Mop53BP1 and microtubule proteins, not only in the mitosis process but also in other cell functions as the organization of intracellular structure and intracellular transport.

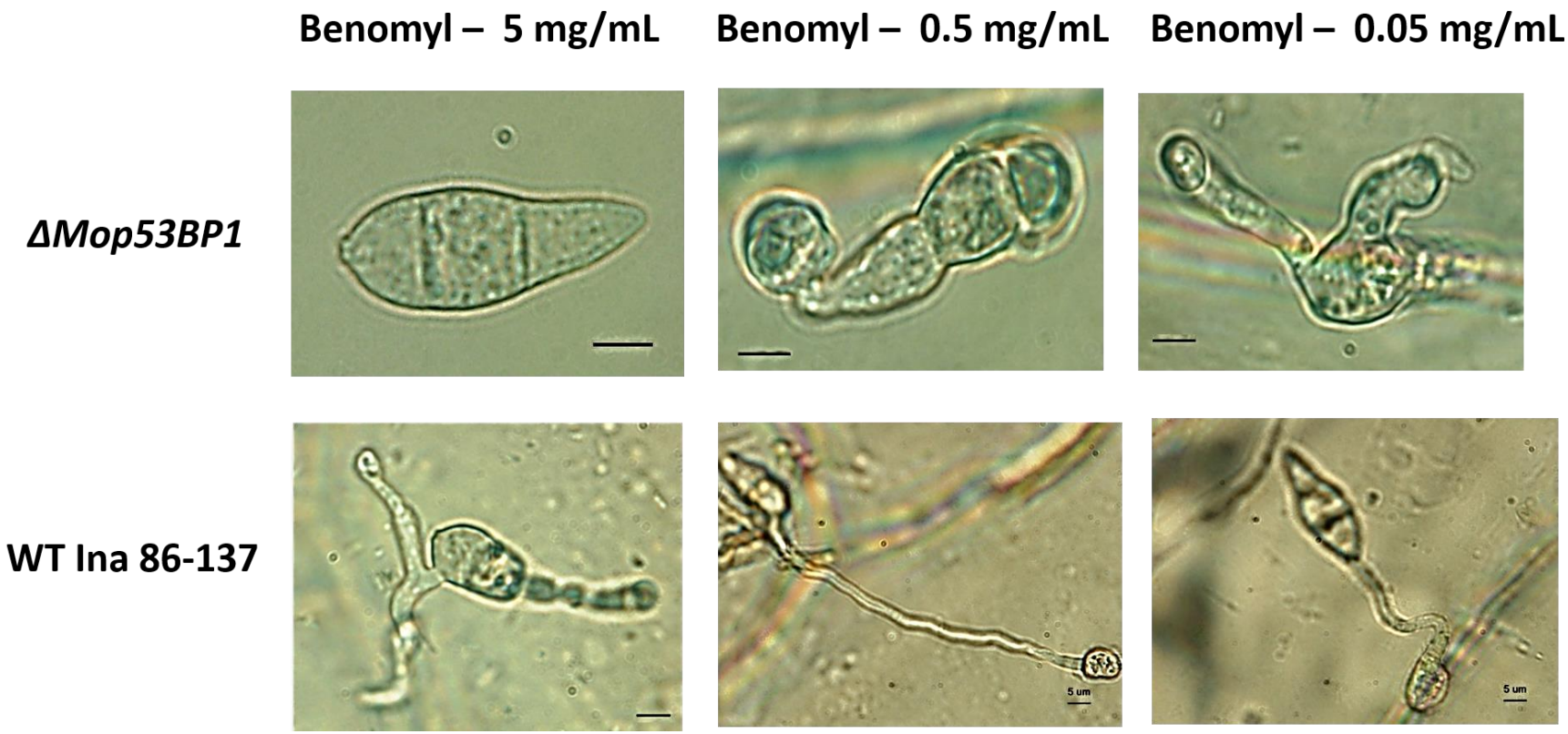

Figure 19. Appressorium development of wild-type and *ΔMop53BP1* mutant exposed to different concentrations of the microtubule inhibitor benomyl. Deletion mutant showed hypersensitivity to the microtubule inhibitor in all assays forming abnormal and multiple appressoria. Wild-type could develop normal appressorium in the lowest concentration of benomyl. Scale bar = 5 μm.

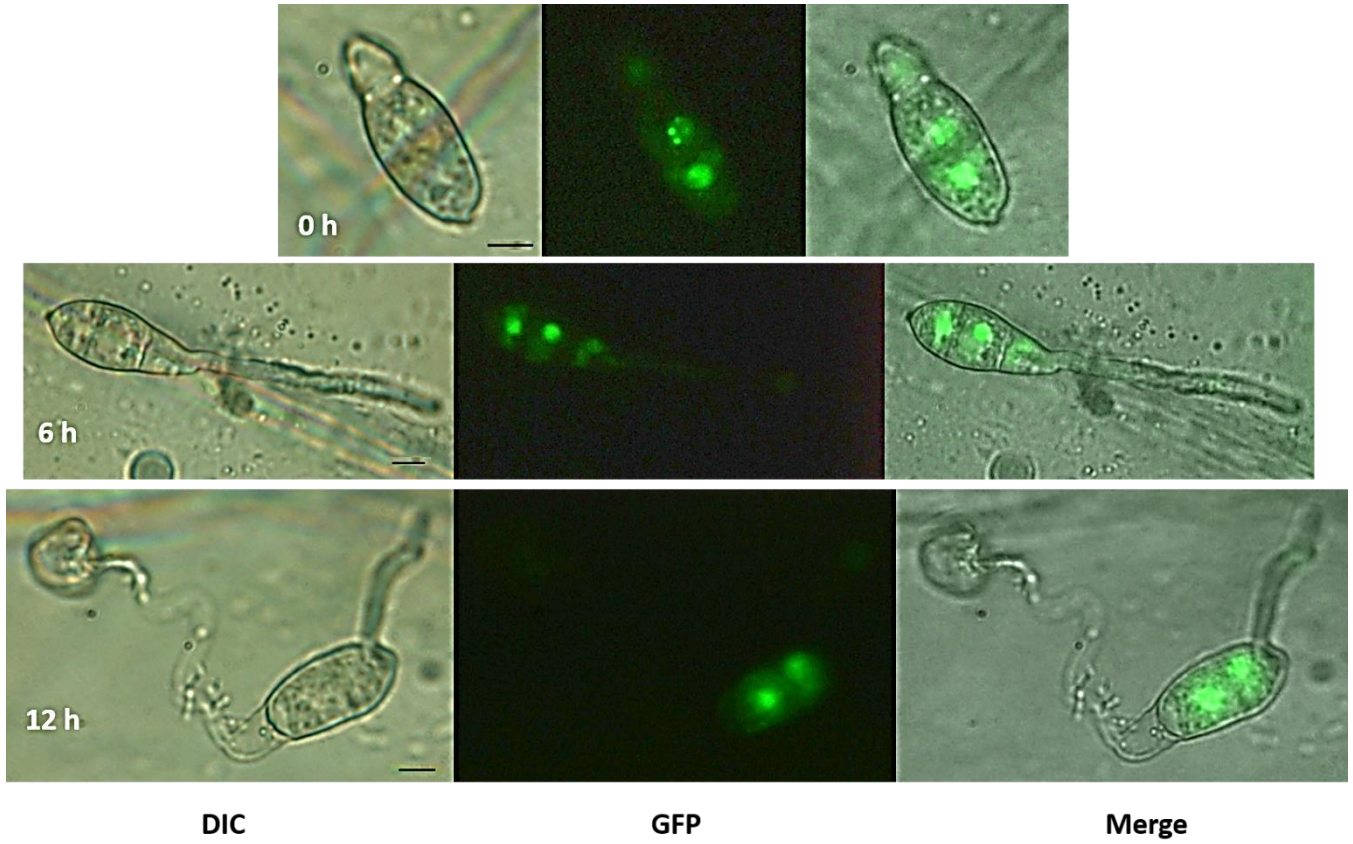

Figure 20. Effect of Benomyl on appressoria development. Overexpression mutant presented some resistance to benomyl following exposure to 5 mg/mL, observed at 0h, 6h, and 12h.

12 h

24 h

Figure 21. Effect of Benomyl on appressoria development. WT development following exposure to benomyl (5 mg/mL−1), observed at 12 h and 24 h. Scale bar = 5 μm.

Discussion

Tubulins play a central role in several cellular processes; cell divisions, intracellular transports, and the establishment of cell polarity (Hu et al. 2015). Regarding appressorium formation, Takano et al. (2001) demonstrated that microtubules are vital to a precise postmitotic nuclei distribution during appressorium formation of *Colletotrichum lagenarium*. In our study, the deletion mutants of *Mop53BP1* presented an elevated number of appressoria and reduced virulence, which could be a consequence of a disturbed tubulin function, affecting the nuclei distribution. Similarly, Luo et al. (2014) reported that deletions of FgKin1 and MoKin1, a kinase that regulates the localization of β-tubulins in *Fusarium graminearum* and *Magnaporthe oryzae* respectively, resulted in reduced virulence and defects in ascospore germination and release. Also, when Hu et al. (2015) deleted the α-tubulin encoding gene *FaTUA1* in *Fusarium asiaticum*, the mutants showed reduced mycelial growth, twisted hyphae, abnormal nuclei, decrease in conidiation and abnormal conidia.

In summary, the targeted deletion of *Mop53BP1* had strong effects on appressorium formation and pathogenicity of *P. oryzae* to rice. The next chapter will be directed at studying Mop53BP1 functions and interactions with other proteins as α, β, and γ tubulins.

Table 2. Synthetic oligonucleotides used in the overexpression of Mop53BP1.

Primer name	**Sequence (5'-3')**	**Target gene**	**Application**
TEFf	AGCAAACGGTGGTCAAAG	TEF promoter region	GFP-*Mop53BP1* overexpression
TEFr	GACGGTTGTGTATGGAAG	TEF promoter region	GFP-*Mop53BP1* overexpression
Invfwr	ATGGTGAGCAAGGGCGAGGAG	Start of GFP-*Mop53BP1*	Inverse PCR for GFP-*Mop53BP1* overexpression
Invrev	AAGGTGGGCATGTCATATCTTTCACC	Start of *Mop53BP1* promoter	Inverse PCR for GFP-*Mop53BP1* overexpression
TEFovf	TGACATGCCCACCTTAGCAAACGGTGGTCAAAG	TEF1 promoter	GFP-*Mop53BP1* overexpression
TEFovr	GCCCTTGCTCACCATGACGGTTGTGTATGGAAG	TEF1 promoter	GFP-*Mop53BP1* overexpression

CHAPTER FOUR

Visualization and expression of α-Tubulin in Mop53BP1 deletion mutants

Chapter 4

4. Visualization and expression of α-Tubulin in *P. oryzae* deletion mutants

4.1. Evaluating the relationship between Mop53BP1 and α-Tubulin

In order to visualize the tubulin dynamics in the presence and absence of Mop53BP1, we construct a TEF1$_{::}$mCherry::Tuba plasmid by fusing mCherry to the N-terminus of α-tubulin gene, using the constitutive promoter TEF1. With this strategy, it was possible to observe the role of microtubules during the appressorium formation of wild-type and *ΔMop53BP1* mutants.

Material and Methods

4.1.1. Construction of pBLASTR-DEST-TEF::mCherry::Tuba plasmid and transformation

Firstly, in order to replace the eGFP for the mCherry fluorescent protein we opened the vector pENTR- TEF1$_{::}$eGFP::*Mop53BP1* (from section 3.1.1) by inverse PCR using the primers TEFr and Mop53BP1F (Table 3). After that, the mCherry fragment was amplified using the overlapping pair of primers RFPovf and RFPovr (Table 3). The products of inverse and overlapping PCR were fused using NEBuilder® HiFi DNA Assembly kit. Thus, the vector pENTR-TEF1$_{::}$mCherry:: *Mop53BP1*was opened again by inverse PCR using the primers InvTubaF and TEFr.

The tubulin alpha chain gene (MGG_11412) was amplified from Ina 86-137 cDNA using the primers Tubaf and Tubar (Table 3). Subsequently, the reaction product was purified and used as a template for a new amplification using the overlapping pair of primers Tubaovrf and Tubaovrev (Table 3) (tubulin alpha chain gene sequence was checked by sequence reaction).

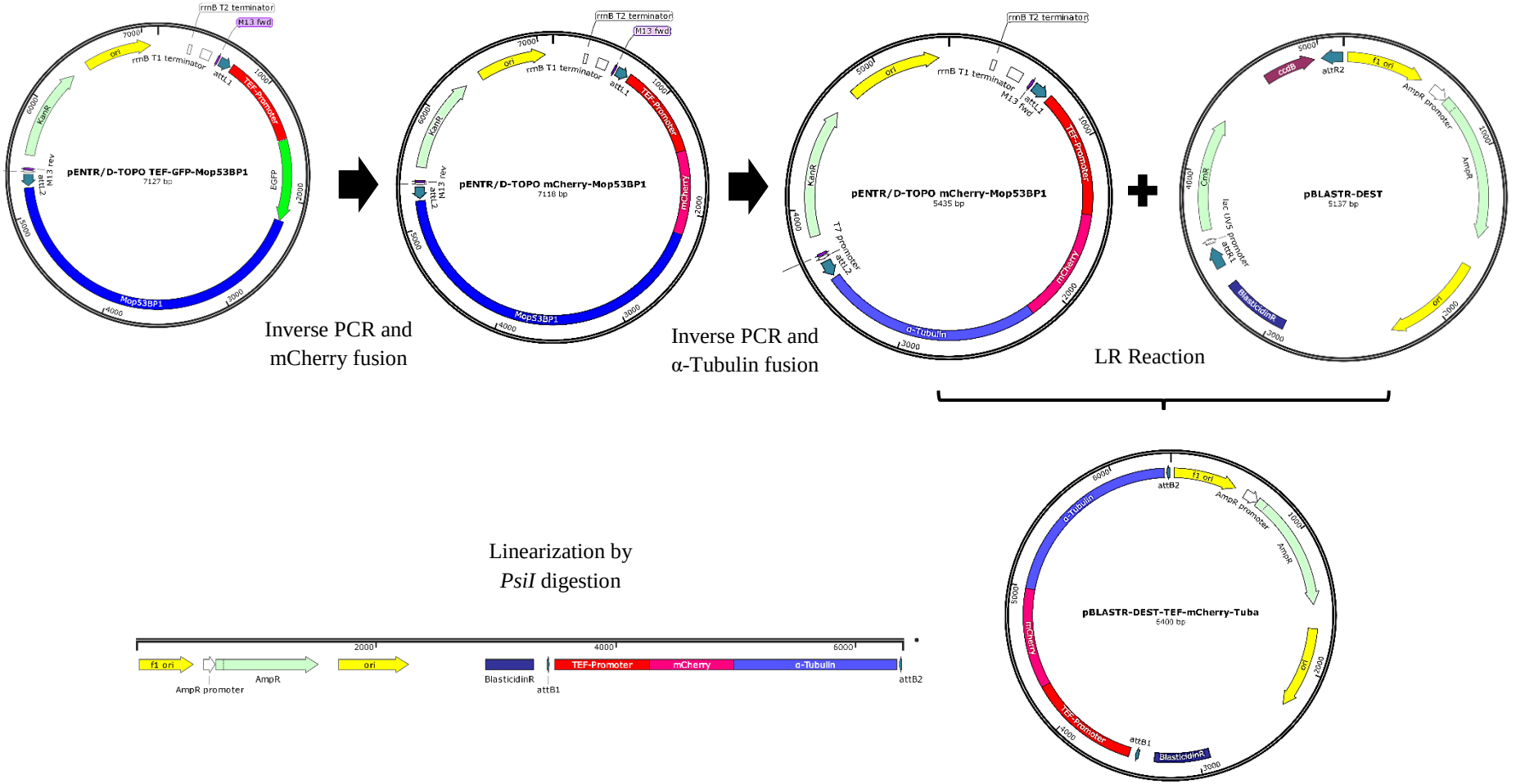

Figure 22. Construction of pBLASTR-DEST-TEF::mCherry::Tuba plasmid. The destination vector was linearized with *PsiI* and used to transform INA86-137 *Mop53BP1* wild-type and disruption mutants.

The products of inverse and overlapping PCR were fused using NEBuilder® HiFi DNA Assembly kit. The pENTR-TEF1$_{::}$mCherry::Tuba was then transferred to the blasticidin S-resistant pBLASTR- TEF1$_{::}$mCherry::Tuba via a LR reaction using Gateway LR Clonase II Enzyme mix (Invitrogen, Life Technologies Japan Ltd., Tokyo, Japan) (Fig. 22). Similar to section 2.2.1 and 2.2.2, the pBLASTR- TEF1$_{::}$mCherry::Tuba plasmid was linearized using *PsiI* restriction enzyme and transformed into INA86-137 wild-type and *Mop53BP1* disruption mutant. The verification of positive transformants was performed according to section 2.2.3 (the conditions of all PCR reactions are listed in Appendix-I).

4.1.2. Appressorium induction using hydrophobic microscope glass slides

Conidia suspensions of *P. oryzae* confirmed mutants were inoculated on hydrophobic microscope glass slides, and mCherry fluorescence observations during appressorium development were performed according to section 2.2.4, using the filter set Cy3^{TM} - Olympus.

Results

After PCR and Southern Hybridization confirmation (Fig. 23), the cellular localization of α-Tubulin was assessed on conidia, germ tube and appressorium formation of *TUBA1, TUBA2* (resulting from the transformation using WT strain)*, ΔMop53BP1-TUB1* and (resulting from the transformation using *ΔMop53BP1* strain) mutants.

The expression of α-Tubulin tagged to mCherry protein was low during all stages of appressorium formation, exceptionally after 6 hours, in the germ tube stage of the wild-type *TUBA1* strain (Fig. 24). This step of appressorium formation comprises the mitosis process, which requires the presence of tubulins for microtubule polymerization.

However, no fluorescence was detected in the deletion mutant (Fig. 25) supporting the hypothesis that Mop53BP1 may interact with α-Tubulin during the mitosis of appressorium formation.

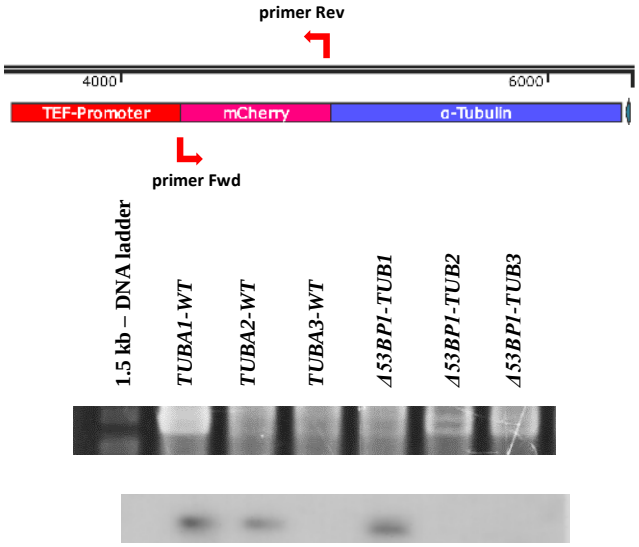

Figure 23. Confirmation of positive transformants by PCR and Southern hybridization. PCR with primers RFPovf and RFPovr (Table 2), and Southern hybridization by digesting genomic DNA with PsiI and EcoRI and using mCherry fragment as a probe.

Figure 24. Expression of the mCherry-αTubulin fusion under the control of TEF1 promoter during appressorium formation of the wild-type strain. Fluorescence observed after 6 hours of growth. Scale bar = 5 μm.

Figure 25. Expression of the mCherry-αTubulin fusion under the control of TEF1 promoter during appressorium formation of *ΔMop53BP1* strain. Fluorescence signals were undetected during all steps of appressorium development. Scale bar = 5 μm.

Discussion

The expression of α-Tubulin tagged to mCherry protein was detected only in the germ tube stage of the wild-type *TUBA1* strain, supporting the hypothesis that Mop53BP1 may interact with α-Tubulin during the mitosis of appressorium formation.

Despite consistent result regarding α-Tubulin expression in the wild-type and *ΔMop53BP1* mutant, the fluorescence signal was weak during the microscope observations. The fusion between tubulins proteins and fluorescent markers as GFP or mCherry has been performed in phytopathogenic fungi, Takano et al. (2001) analyzed the microtubule dynamics during appressorium formation of *Colletotrichum lagenarium*. The authors reported that the strain expressing the fusion protein (a-tubulin genes of *C. lagenarium* tagged to GFP) formed fluorescent filaments during all steps of fungi growth, and at the nuclear division, mitotic spindles appeared showing a high fluorescence intensity. The same tubulin dynamic was reported by Saunders et al. (2010) when the expression of β-tubulin tagged to GFP was evaluated during appressorium formation of *M. oryzae*. According to the authors, the mitosis occurs 4 to 6 h with an influx of b-tubulin:GFP into the nucleus as the spindle is formed, consequently a high fluorescence is detected in the conidia cell that would generate the appressorium.

A similar result was presented in this study; a high mCherry fluorescence was detected after 6 hours of appressorium development, however during the other steps the fluorescence was undetected. Therefore, future efforts will be directed towards to improve the mCherry- α-Tubulin expression in *P. oryzae*. A possible strategy could be the usage of a different promoter; Takano et al. (2001) expressed the GFP-α-Tubulin under the control of SCD1 promoter, responsible for encoding the scytalone dehydratase involved in the production of fungal dihydroxynaphthalene melanin, which is crucial for appressorium development. A second approach is similar to the work conducted by

Saunders et al. (2010), who expressed the b-tubulin:GFP from *Neurospora crassa*, a model filamentous fungus whose genes are often used in heterologous expression.

Table 3. Synthetic oligonucleotides used in the expression of α-Tubulin tagged to mCherry in *P. oryzae*.

Primer name	**Sequence (5'-3')**	**Target gene**	**Application**
Mop53BP1F	ATGGCTAAGAAGAAGGCAAAACCAA	*Mop53BP1* ORF	Inverse PCR – open plasmid
TEFr	GACGGTTGTGTATGGAAG	TEF promoter region	Inverse PCR – open plasmid
RFPovf	CCATACACAACCGTCATGGTGAGCAAGGGCGAGG	mCherry fragment	mCherry fusion
RFPovr	CTTCTTCTTAGCCATCTTGTACAGCTCGTCCATGCC	mCherry fragment	mCherry fusion
Tubaf	TGACATGCCCACCTTAGCAAACGGTGGTCAAAG	α-Tubulin fragment	Overexpression of α-Tubulin
Tubar	GCCCTTGCTCACCATGACGGTTGTGTATGGAAG	α-Tubulin fragment	Overexpression of α-Tubulin
Tubaovrf	GACGAGCTGTACAAGATGAAAGGCGAGGTCCTT	α-Tubulin fragment	Overexpression of α-Tubulin
Tubaovrev	TCCATCTCCTCTGCTCTAGTACTCGGCATCACC	α-Tubulin fragment	Overexpression of α-Tubulin

CHAPTER FIVE

Summary

Chapter 5

Summary

Analysis of the DNA damage signal transducer ortholog Mop53BP1 in Pyricularia oryzae

Pyricularia oryzae (teleomorph: *Magnaporthe oryzae*) is the causal agent of the rice blast, the most important disease that affects rice production worldwide. In addition, during the last decades, the blast fungus emerged as an explosive threat to wheat production, causing up to 100% yield losses (Cruz and Valent 2017).

To gain entry into host plant, *P. oryzae* develops a specialized structure called appressorium, this dome-shaped, rich in chitin and melanized structure generates osmotic pressure by accumulation of glycerol and applies mechanical pressure to breach the leaf surface, growing invasively into the first epidermal cells by means of invasive hyphae (Wilson and Talbot 2009).

During the last years, it was evidenced that cell cycle regulation provides control points for infection structure development in *P. oryzae.* It was also demonstrated that proper mitosis is necessary for appressorium formation and followed by conidial autophagy, which are essential for the successful plant infection. The key steps for the initiation and completion of appressorium formation in *P. oryzae* are the entry into S-phase and mitosis, respectively (Saunders et al. 2010). These analyses had been performed using mutants for mitosis and chemical inhibitors for DNA synthesis and microtubule function.

An ortholog gene for p53BP1, a signal transducer protein that participates in G2-M cell cycle checkpoint in higher eukaryotes, had been identified in the genome of *P.*

oryzae. Also, the deletion mutants of Mop53BP1 formed multiple abnormal appressoria per conidia and were unable to develop pathogenicity (Tashika et al. unpublished data).

Therefore, the main objective of this work was to clarify the importance of *Mop53BP1* during appressorium formation by means of gene expression analysis and studying the relationship of Mop53BP1 with proteins related to cell cycle progression.

To test the response to DNA damage agents and for a better understanding of the physiological function of *Mop53BP1*, the expression of this gene was evaluated in wild-type strains cultured in liquid media with DNA damaging agents. qRT-PCR analyzes showed that the expression of *Mop53BP1* was low for all treatments suggesting that this gene does not have a crucial role in the vegetative growth and DNA double-strand break repair of *P. oryzae*. Similar to these results, the deletion of ortholog *Hsr-9* from *C. elegans* did not affect post-embryonic development after γ-ray treatment, and *hsr-9* mutations did not prevent the cell cycle arrest induced by DSBs (Ryu et al. 2013).

In order to visualize the location and study the expression of Mop53BP1 during the appressorium differentiation, we fused the green fluorescent protein (eGFP) to Mop53BP1 and conducted a microscopic observation of different stages of appressorium development. Fluorescence signals were detected in nuclei regions of conidia and in the initial germ tube stage. Also, qRT-PCR analyzes revealed that *Mop53BP1* expression was highest at the initial point and decreased according to appressorium development. Then we first inferred that Mop53BP1 is expressed in the first hours of appressorium formation and is might working during cell cycle checkpoints G1/G2/M. Our first hypothesis was that Mop53BP1 was interacting with Serine/threonine-protein kinase Chk1, similar to Crb2 from *S. pombe* (Saka et al. 1997). Chk1 is responsible for mediating the Inhibitory phosphorylation of B-type cyclin–CDK1, and consequently, arrest the cell cycle during DNA damage or in the presence of unreplicated chromatin (Osés-Ruiz et al. 2016).

To study the influence of *Mop53BP1* overexpression during the appressorium formation, we replaced the native promoter by the constitutive TEF1 gene promoter region generating a TEF1-GFP-Mop53BP1 mutant. Thus, a strong fluorescence was observed in the nuclei during all the stages of appressorium formation. Also, these mutants produced normal appressorium and infection structures, suggesting that Mop53BP1 overexpression did not affect the appressorium development and that the protein localizes to nuclei during all steps of plant infection.

In order to clarify whether Mop53BP1 is related to G1/S, G2/M checkpoints, we observed the appressorium formation of wild-type, *ΔMop53BP1* and overexpression mutants in the presence of DNA synthesis inhibitor hydroxyurea (HU) and microtubule inhibitor benomyl. In the presence of HU, the cell cycle progression was arrested in wild-type and deletion mutants, showing that Mop53BP1 is not participating in the DNA replication checkpoint. However, *Mop53BP1* null mutants displayed hypersensitivity to benomyl, while overexpression mutants showed some resistance to the microtubule inhibitor. Several cases of resistance to benomyl and other benzimidazole fungicides have been reported (e.g. Yang et al. 2015; Liu et al. 2014; Fan et al. 2014; Zhang et al. 2010; Chung et al. 2010) in most cases, the resistance is associated with point mutations in β-tubulin gene which result in altered amino acid sequences at the benzimidazole binding site. These evidences contribute to another hypothesis that Mop53BP1 may interact with microtubule proteins as α, β, and γ tubulins during appressorium formation.

To visualize the tubulin dynamics in the presence and absence of Mop53BP1, we fused the mCherry fluorescent protein to α-Tubulin using the constitutive promoter TEF1. The fluorescence was low during all stages of appressorium formation, exceptionally after 6 hours, in the germ tube stage of the wild-type strain. This step of appressorium formation comprises the mitosis process, which requires the presence of tubulins for

microtubule polymerization. However, no fluorescence was detected in the deletion mutant supporting the hypothesis that Mop53BP1 may interact with α-Tubulin during the mitosis of appressorium formation.

Taken together, this thesis revealed that Mop53BP1 has an important role in nuclear division and distribution in *P. oryzae*, via interaction with microtubules. In addition, this thesis first uncovered the role of microtubule in the initiation of appressorium formation. These knowledge should contribute to further understanding of appressorium formation in *P. oryzae*, which is an important target for the disease control.

CHAPTER SIX

References

A Schamber, M Leroch, J Diwo, K Mendgen, M Hahn (2010) The role of mitogen-activated protein (MAP) kinase signaling components and the Ste12 transcription factor in germination and pathogenicity of *Botrytis cinereal*. Mol Plant Pathol 11:105–119

Abe A, Elegado E, Sone T (2006) Construction of pDESTR, a GATEWAY vector for gene disruption in filamentous fungi. Curr Microbiol 52:210–215

Botuyan MV, Lee J, Ward IM, Kim JE, Thompson JR, Chen J, Mer G (2006) Structural basis for the methylation state-specific recognition of histone H4-K20 by 53BP1 and Crb2 in DNA repair. Cell 127:1361-73

Chang HX, Miller LA, Hartman GL (2014) Melanin-independent accumulation of turgor pressure in appressoria of Phakopsora pachyrhizi. Phytopathology 104:977-84

Chung WH, Chung WC, Peng MT, Yang HR, Huang JW (2010) Specific detection of benzimidazole resistance in *Colletotrichum gloeosporioides* from fruit crops by PCR-RFLP. New Biotechnol 27:17-24

Cruz CD, Valent B (2017) Wheat blast disease: danger on the move. Tropical Plant Pathology 1-3

Derbyshire DJ, Basu BP, Serpell LC, Joo WS, Date T, Iwabuchi K, Doherty AJ (2002) Crystal structure of human 53BP1 BRCT domains bound to p53 tumor suppressor. EMBO J 21:3863-72

DiTullio RA, Mochan TA, Venere M, Bartkova J, Sehested M, Bartek J, Halazonetis TD (2002) 53BP1 functions in an ATM-dependent checkpoint pathway that is constitutively activated in human cancer. Nature Cell Biol 4:998-1002

Du LL, Nakamura TM, Moser BA, Russell P (2003) Retention but not recruitment of Crb2 at double-strand breaks requires Rad1 and Rad3 complexes. Mol Cell Biol 23:6150-6158

Fan J, Luo Y, Michailides TJ, Guo L (2014) Simultaneous quantification of alleles E198A and H6Y in the β-tubulin gene conferring benzimidazole resistance in *Monilinia fructicola* using a duplex real-time (TaqMan) PCR. Pest Manag Sci 70:245-251

Fernandez-Capetillo O, Chen HT, Celeste A, Ward I, Romanienko PJ, Morales JC, Naka K, Xia Z, Camerini-Otero RD, Motoyama N, Carpenter PB (2002) DNA damage-induced G2–M checkpoint activation by histone H2AX and 53BP1. Nature Cell Biol 4:993-997

Franck WL, Gokce E, Oh Y, Muddiman DC, Dean RA (2013) Temporal analysis of the Magnaporthe oryzae proteome during conidial germination and cyclic AMP (cAMP)-mediated appressorium formation. Molecular & Cellular Proteomics 12: 2249-2265

Hsu LC, Doan TP, White RL (2001) Identification of a γ-tubulin-binding domain in BRCA1. Cancer Res 61:7713-7718

Hu W, Zhang X, Chen X, Zheng J, Yin Y, Ma Z (2015) α1-Tubulin FaTuA1 plays crucial roles in vegetative growth and conidiation in *Fusarium asiaticum*. Res Microbiol 166: 132-142

Jakob B, Splinter J, Durante M, Taucher-Scholz G (2009) Live cell microscopy analysis of radiation-induced DNA double-strand break motion. Proc Natl Acad Sci 106:3172-3177

Jullien D, Vagnarelli P, Earnshaw WC, Adachi Y (2002) Kinetochore localization of the DNA damage response component 53BP1 during mitosis. J Cell Sci 115:71-9

Kou Y, Naqvi NI (2016) Surface sensing and signaling networks in plant pathogenic fungi. Seminars in cell & developmental biology 57:84-92

Lanver D, Berndt P, Tollot M, Naik V, Vranes M, Warmann T, Münch K, Rössel N, Kahmann R (2014) Plant surface cues prime *Ustilago maydis* for biotrophic development. PLoS Pathogens. 10:e1004272

Li G, Zhou X, Xu JR (2012) Genetic control of infection-related development in *Magnaporthe oryzae*. Curr Opin Microbiol 15:678-684

Liu XH, Chen SM, Gao HM, Ning GA, Shi HB, Wang Y, Dong B, Qi YY, Zhang DM, Lu GD, Wang ZH (2015) The small GTPase MoYpt7 is required for membrane fusion in autophagy and pathogenicity of Magnaporthe oryzae. Env Microbiol. 17:4495-510

Liu Y, Chen X, Jiang J, Hamada MS, Yin Y, Ma Z (2014) Detection and dynamics of different carbendazim-resistance conferring β-tubulin variants of *Gibberella zeae* collected from infected wheat heads and rice stubble in China. Pest Manag Sci 70: 1228-1236

Ludwig N, Löhrer M, Hempel M, Mathea S, Schliebner I, Menzel M, Kiesow A, Schaffrath U, Deising HB, Horbach R (2014) Melanin is not required for turgor generation but enhances cell-wall rigidity in appressoria of the corn pathogen *Colletotrichum graminicola*. Molecular Plant-Microbe Interactions 27:315-27

Luo Y, Zhang H, Qi L, Zhang S, Zhou X, Zhang Y, Xu JR (2014) FgKin1 kinase localizes to the septal pore and plays a role in hyphal growth, ascospore germination, pathogenesis, and localization of Tub1 beta-tubulins in *Fusarium graminearum*. New Phytol 204:943-954

Ndindeng SA, Miki S, Abe A, Asano K, Sone T (2010) EGFP-Rhm51 foci enable the visualization and enumeration of DNA double-strand breaks in *Magnaporthe oryzae*. J. Gen. Plant Pathol 76:377-381

NJ Jenczmionka, FJ Maier, AP Losch, W Schafer (2003) Mating, conidiation and pathogenicity of *Fusarium graminearum*, the main causal agent of the head-blight disease of wheat, are regulated by the MAP kinase gpmk1. Curr Genet 43:87–95

Olivier M, Hollstein M, Hainaut P (2010) TP53 mutations in human cancers: origins, consequences, and clinical use. Cold Spring Harbor perspectives in biology. 2(1):a001008.

Osés-Ruiz M, Sakulkoo W, Littlejohn GR, Martin-Urdiroz M, Talbot NJ (2016) Two independent S-phase checkpoints regulate appressorium-mediated plant infection by the rice blast fungus *Magnaporthe oryzae*. Proc Natl Acad Sci 114:237-244

Panier S, Boulton SJ (2014) Double-strand break repair: 53BP1 comes into focus. Nat Rev Mol Cell Biol 15:7-18

Pérez-Martín J, Bardetti P, Castanheira S, de la Torre A, Tenorio-Gómez M (2016) Virulence-specific cell cycle and morphogenesis connections in pathogenic fungi. Seminars in cell & developmental biology 57:93-99

Rappold I, Iwabuchi K, Date T, Chen J (2001) Tumor suppressor p53 binding protein 1 (53BP1) is involved in DNA damage–signaling pathways. J Cell Biol 153:613-620

Ryder LS, Talbot NJ (2015) Regulation of appressorium development in pathogenic fungi. Current opinion in plant biology 31:8-13

Ryu JS, Kang SJ, Koo HS (2013) The 53BP1 homolog in *C. elegans* influences DNA repair and promotes apoptosis in response to ionizing radiation. PloS One 8:e64028.

Saka Y, Esashi F, Matsusaka T, Mochida S, Yanagida M (1997) Damage and replication checkpoint control in fission yeast is ensured by interactions of Crb2, a protein with BRCT motif, with Cut5 and Chk1. Genes Dev 11:3387-3400

Saunders DGO, Aves SJ, Talbot NJ (2010) Cell Cycle–Mediated Regulation of Plant Infection by the Rice Blast Fungus. Plant Cell 22:497-507

Soanes DM, Chakrabarti A, Paszkiewicz KH, Dawe AL, Talbot NJ (2012) Genome-wide Transcriptional Profiling of Appressorium Development by the Rice Blast Fungus *Magnaporthe oryzae*. PLoS Pathog 8:e1002514

Starita LM, Machida Y, Sankaran S, Elias JE, Griffin K, Schlegel BP, Gygi SP, Parvin JD (2004) BRCA1-dependent ubiquitination of γ-tubulin regulates centrosome number. Mol Cel Biol, 24:8457-8466

Takano Y, Oshiro E, Okuno T (2001) Microtubule dynamics during infection-related morphogenesis of *Colletotrichum lagenarium*. Fungal Genet Biol 34:107-121

Veneault-Fourrey C, Barooah M, Egan M, Wakley G, Talbot NJ (2006) Autophagic fungal cell death is necessary for infection by the rice blast fungus. Science. 312:580-3

Wang B, Matsuoka S, Carpenter PB, Elledge SJ (2002) 53BP1, a mediator of the DNA damage checkpoint. Science 298:1435-1438

Wang GL, Valent B (2017) Durable resistance to rice blast. Science. 355:906-7

Wilson RA, Talbot NJ (2009) Under pressure: investigating the biology of plant infection by *Magnaporthe oryzae*. Nat Rev Micro 7:185-95

Yang F, Abdelnabby H, Xiao Y (2015) Novel point mutations in [beta]-tubulin gene for carbendazim resistance maintaining nematode pathogenicity of *Paecilomyces lilacinus*. Eur J Plant Pathol 143:57

Yoshiyama KO, Sakaguchi K, Kimura S (2013) DNA damage response in plants: conserved and variable response compared to animals. Biology 2:1338-56

Zhang CQ, Liu YH, Zhu GN (2010) Detection and characterization of benzimidazole resistance of *Botrytis cinerea* in greenhouse vegetables. Eur J Plant Pathol 126:509-515

APPENDICES

APPENDIX I: REACTION CONDITIONS AND COMPOSITION OF SOLUTIONS

Reverse-transcription polymerase chain reaction (RT-PCR) – Expression analysis

Component	**Volume**
2x Reaction Mix	25 µL
Template RNA (.01 pg to 1 µg)	x
Sense primer (10 µM)	1 µL
Anti-sense primer (10 µM)	1 µL
SuperScript™ III RT/Platinum™ Taq Mix	2 µL
Autoclaved distilled water	to 50 µL

PCR conditions
55 ^{0}C, 30 min
94 ^{0}C, 2 min
94^{0}C, 15 sec
55 ^{0}C, 55 sec
68 ^{0}C, 3 min
68 ^{0}C, 5 min
4 ^{0}C, ∞

cDNA synthesis reaction

Component	**Volume**
5x VILO™ Reaction Mix	4 µL
10x SuperScript™ Enzyme Mix	2 µL
RNA (up to 2.5 µg)	x µL
DEPC-treated water to	20 µL

Contents were incubated at 25 °C for 10 minutes. Subsequently, the temperature was raised to 42 °C for 60 minutes, and the reaction was terminated at 85 °C for 5 minutes.

Quantitative real-time PCR with SYBR® Green using the StepOnePlus™ Real-Time PCR Systems

Component	**Volume**
SYBR® Green PCR Master Mix	12.5 µL
Forward primer, 10 ρM	0.5 µL
Reverse primer, 10 ρM	0.5 µL
Template (10^2-10^9 copies of plasmid)	1 µL
DEPC-treated water to	25 µL

PCR conditions
Step 1, 50 °C, 2 min, (Rep 1)
Step 2, 95 °C, 10 min
95 °C, 15 sec (Rep 1)
Step 3, 60 °C, 1 min (Rep 40)

Amplification of $P_{Mop53BP1}$*Mop53BP1* ***KOD-FX***

Component	**Volume**
2x PCR buffer for KOD FX	25 µL
DNTPs 2mM	10 µL
Sense primer (10 µM)	1.5 µL
Anti-sense primer (10 µM)	1.5 µL
Template DNA	≤50 ng / 50 µL
KOD FX (1.0U/µL)	1 µL
Autoclaved distilled water	to 50 µL

PCR conditions
3-step cycle
Pre-denaturation: 94 °C, 2 min.
Denaturation: 98 °C,10 sec. *
Annealing: 55 °C, 30 sec. *
Extension: 68 °C, 2 min*
* 35 cycles

pENTR™/D-TOPO® Cloning Procedure

Component	**Volume**
Fresh PCR product	0.5–4 µL
TOPO® vector	1 µL
Water to a final volume of	5 µL

2:1 molar ratio of PCR product: TOPO® vector.

Inverse PCR to open pENTR- $P_{Mop53BP1}$***Mop53BP1 plasmid***

Component	**Volume**
2x PCR buffer for KOD FX	25 µL
DNTPs 2mM	10 µL
Sense primer (10 µM)	1.5 µL
Anti-sense primer (10 µM)	1.5 µL
Template DNA	≤50 ng / 50 µL
KOD FX (1.0U/µL)	1 µL
Autoclaved distilled water	to 50 µL

PCR conditions
3-step cycle
Pre-denaturation: 94 °C, 2 min.
Denaturation: 98 °C,10 sec. *
Annealing: 55 °C, 30 sec. *
Extension: 68 °C, 3 min 15 sec *
* 35 cycles

Amplification of eGFP fragment by KOD-FX

Component	**Volume**
2x PCR buffer for KOD FX	25 µL
DNTPs 2mM	10 µL
Sense primer (10 µM)	1.5 µL
Anti-sense primer (10 µM)	1.5 µL
Template DNA	≤50 ng / 50 µL
KOD FX (1.0U/µL)	1 µL
Autoclaved distilled water	to 50 µL

PCR conditions
3-step cycle
Pre-denaturation: 94 °C, 2 min.
Denaturation: 98 °C,10 sec. *
Annealing: 55 °C, 30 sec. *
Extension: 68 °C, 42 sec*
* 35 cycles

Ligation between pENTR-$P_{Mop53BP1}$Mop53BP1 and Kinated GFP

Component	**Volume**
pENTR-$P_{Mop53BP1}$Mop53BP1 plasmid	1 µL
Kinated GFP	5 µL
10x ligation buffer	1 µL
T4 ligase (NEB)	1 µL
Autoclaved distilled water	to 10 µL
Reaction incubated overnight	

LR reaction to obtain pBLASTR-DEST $P_{Mop53BP1}$eGFP::Mop53BP1

Component	**Volume**
pENTR-$P_{Mop53BP1}$eGFP::Mop53BP1 plasmid (100-300 ng)	1-10 µl
Destination vector- pBLASTR-DEST (150 ng/µl)	2 µl
LR Clonase™ reaction buffer	4 µl
TE Buffer, pH 8.0	to 16 µl

PCR for positive transformants - $P_{Mop53BP1}$::eGFP::Mop53BP1

Component	**Volume**
2x PCR buffer for KOD FX	25 µL
DNTPs 2mM	10 µL
Sense primer (10 µM)	1.5 µL
Anti-sense primer (10 µM)	1.5 µL
Template DNA	≤50 ng / 50 µL
KOD FX (1.0U/µL)	1 µL
Autoclaved distilled water	to 50 µL

PCR conditions

3-step cycle
Pre-denaturation: 94 °C, 2 min.
Denaturation: 98 °C,10 sec. *
Annealing: 55 °C, 30 sec. *
Extension: 68 °C, 2 min 2 sec*
* 35 cycles

Hind III HF® and EcoRI HF® digestion

C**omponent**	**Volume**
DNA	1 µg
10X CutSmart Buffer	5 µl (1X)
EcoRI-HF	1.0 µl
HindIII-HF	1.0 µl
Nuclease-free Water	to 50 µl

Reaction incubated at 37°C for 1 hour.

PsiI digestion

C**omponent**	**Volume**
DNA	1 µg
10X CutSmart Buffer	5 µl
PsiI	1.0 µl
Nuclease-free Water	to 50 µl

Reaction incubated at 37°C for 1 hour.

Inverse PCR to open pENTR-P$_{Mop53BP1}$eGFP::Mop53BP1 plasmid

C**omponent**	**Volume**
2x PCR buffer for KOD FX	25 µL
DNTPs 2mM	10 µL
Sense primer (10 µM)	1.5 µL
Anti-sense primer (10 µM)	1.5 µL
Template DNA	≤50 ng / 50 µL
KOD FX (1.0U/µL)	1 µL
Autoclaved distilled water	to 50 µL

PCR conditions
3-step cycle
Pre-denaturation: 94 °C, 2 min.
Denaturation: 98 °C,10 sec. *
Annealing: 55 °C, 30 sec. *
Extension: 68 °C, 4 min 10 sec*
* 35 cycles

TEF and Overlapping TEF fragment amplification

C**omponent**	**Volume**
2x PCR buffer for KOD FX	25 µL
DNTPs 2mM	10 µL

Sense primer (10 μM)	1.5 μL
Anti-sense primer (10 μM)	1.5 μL
Template DNA	≤50 ng / 50 μL
KOD FX (1.0U/μL)	1 μL
Autoclaved distilled water	to 50 μL

PCR conditions
3-step cycle
Pre-denaturation: 94 °C, 2 min.
Denaturation: 98 °C,10 sec. *
Annealing: 55 °C, 30 sec. *
Extension: 68 °C, 24 sec. *
* 35 cycles

Fusion of TEF Promoter and opened pENTR-$P_{Mop53BP1}$eGFP::Mop53BP1 plasmid

Component	**Volume/Amount**
Total Amount of Fragments	0.03–0.2 pmols
HiFi DNA Assembly Master Mix	10 μl
Autoclaved distilled water	to 20 μL
Recommended DNA Molar Ratio	vector:insert = 1:2

LR reaction to obtain pBLASTR-DEST TEF::eGFP::Mop53BP1

Component	**Volume**
pENTR-TEF::eGFP::Mop53BP1 plasmid (100-300 ng)	1-10 μl
Destination vector- pBLASTR-DEST (150 ng/μl)	2 μl
LR Clonase™ reaction buffer	4 μl
TE Buffer, pH 8.0	to 16 μl

PCR for positive transformants – TEF::eGFP::Mop53BP1

Component	**Volume**
2x PCR buffer for KOD FX	25 μL
DNTPs 2mM	10 μL
Sense primer (10 μM)	1.5 μL
Anti-sense primer (10 μM)	1.5 μL
Template DNA	≤50 ng / 50 μL
KOD FX (1.0U/μL)	1 μL
Autoclaved distilled water	to 50 μL

PCR conditions
3-step cycle
Pre-denaturation: 94 °C, 2 min.
Denaturation: 98 °C,10 sec. *
Annealing: 55 °C, 30 sec. *
Extension: 68 °C, 1 min *
* 35 cycles

KpnI HF® and EcoRI HF® digestion

C**omponent**	**Volume**
DNA	1 µg
10X CutSmart Buffer	5 µl (1X)
EcoRI-HF	1.0 µl
KpnI-HF	1.0 µl
Nuclease-free Water	to 50 µl

Reaction incubated at 37°C for 1 hour.

Inverse PCR to open pENTR-TEF::eGFP::Mop53BP1 plasmid

C**omponent**	**Volume**
2x PCR buffer for KOD FX	25 µL
DNTPs 2mM	10 µL
Sense primer (10 µM)	1.5 µL
Anti-sense primer (10 µM)	1.5 µL
Template DNA	≤50 ng / 50 µL
KOD FX (1.0U/µL)	1 µL
Autoclaved distilled water	to 50 µL

PCR conditions
3-step cycle
Pre-denaturation: 94 °C, 2 min.
Denaturation: 98 °C,10 sec. *
Annealing: 55 °C, 30 sec. *
Extension: 68 °C, 1 min 42 sec*
* 35 cycles

mCherry and Overlapping mCherry fragment amplification

C**omponent**	**Volume**
2x PCR buffer for KOD FX	25 µL
DNTPs 2mM	10 µL
Sense primer (10 µM)	1.5 µL
Anti-sense primer (10 µM)	1.5 µL
Template DNA	≤50 ng / 50 µL
KOD FX (1.0U/µL)	1 µL
Autoclaved distilled water	to 50 µL

PCR conditions
3-step cycle
Pre-denaturation: 94 °C, 2 min.
Denaturation: 98 °C,10 sec. *
Annealing: 55 °C, 30 sec. *
Extension: 68 °C, 21 sec*
* 35 cycles

Fusion of mCherry and opened pENTR-TEF::eGFP::Mop53BP1 plasmid

Component	**Volume/Amount**
Total Amount of Fragments	0.03–0.2 pmols
HiFi DNA Assembly Master Mix	10 µl
Autoclaved distilled water	to 20 µL
Recommended DNA Molar Ratio	vector:insert = 1:2

Inverse PCR to open pENTR-TEF::mCherry::Mop53BP1 plasmid

Component	**Volume**
2x PCR buffer for KOD FX	25 µL
DNTPs 2mM	10 µL
Sense primer (10 µM)	1.5 µL
Anti-sense primer (10 µM)	1.5 µL
Template DNA	≤50 ng / 50 µL
KOD FX (1.0U/µL)	1 µL
Autoclaved distilled water	to 50 µL

PCR conditions
3-step cycle
Pre-denaturation: 94 °C, 2 min.
Denaturation: 98 °C,10 sec. *
Annealing: 55 °C, 30 sec. *
Extension: 68 °C, 2 min*
* 35 cycles

α-Tubulin and Overlapping α-Tubulin fragment amplification

Component	**Volume**
2x PCR buffer for KOD FX	25 µL
DNTPs 2mM	10 µL
Sense primer (10 µM)	1.5 µL
Anti-sense primer (10 µM)	1.5 µL
Template DNA	≤50 ng / 50 µL
KOD FX (1.0U/µL)	1 µL
Autoclaved distilled water	to 50 µL

PCR conditions
3-step cycle
Pre-denaturation: 94 °C, 2 min.
Denaturation: 98 °C,10 sec. *
Annealing: 55 °C, 30 sec. *
Extension: 68 °C, 39 sec*
* 35 cycles

Fusion of α-Tubulin and opened pENTR-TEF::mCherry::Mop53BP1 plasmid

Component	**Volume/Amount**
Total Amount of Fragments	0.03–0.2 pmols
HiFi DNA Assembly Master Mix	10 µL
Autoclaved distilled water	to 20 µL
Recommended DNA Molar Ratio	vector:insert = 1:2

PsiI HF® and EcoRI HF® digestion

Component	**Volume**
DNA	1 µg
10X CutSmart Buffer	5 µl (1X)
EcoRI-HF	1.0 µl
PsiI-HF	1.0 µl
Nuclease-free Water	to 50 µl

Reaction incubated at 37°C for 1 hour.

Sequencing Reaction

Component	**Volume**
Terminator ready Reaction Mix	4 µL
BigDye sequencing Buffer	2 µL
Template (300 ng)	x µL
Primer (3.2 pmol) (50-100 ng)	1 µL
Autoclaved distilled water	to 20 µL

Media

LB-Ampicillin

Polypeptone	10 g/L
Yeast Extract	5 g/L
Sodium Chloride	10 g/L
Fill up with autoclaved distilled water	1 L

Adjust Ph to 7.0

Autoclave at 121^0C for 15 min, allow to cool down to 60^0C, add ampicillin to a final concentration of 100 µg/mL.

LB-Agar/Ampicillin

Polypeptone	10 g/L
Yeast Extract	5 g/L
Sodium Chloride	10 g/L
Fill up with autoclaved distilled water	1 L

Adjust Ph to 7.0

Agar	15 g/L

Autoclave at 121^0C for 15 min, allow to cool down to 60^0C, add ampicillin to a final concentration of 100 µg/mL.

SOC Medium

Solution A	
Tryptone	20 g/L
Yeast extract	5 g/L
Potassium chloride	0.1864 g/L
Sodium chloride	0.5844 g/L
Magnesium chloride hydride	2.033 g/L
Solution B	
Glucose	3.6 g/L

Dissolve A in 900 mL and adjust to pH 7.0, autoclave at 121^0C for 15 min.
Dissolve B in 100 mL and autoclave at 121^0C for 15 min.
Mix A and B after autoclaving.

LB-Agar/Kanamycin

Polypeptone	10 g/L
Yeast Extract	5 g/L
Sodium Chloride	10 g/L
Fill up with autoclaved distilled water	1 L
Adjust Ph to 7.0	
Agar	15 g/L

Autoclave at 121^0C for 15 min, allow to cool down to 60^0C, add kanamycin to a final concentration of 50 μg/mL.

Oatmeal Agar

Oatmeal	50 g/L
Sucrose	20 g/L
Agar	35 g/L

Add oatmeal to water, boil at 95^0C for 30 min and filtrate using a gauze and funnel. Mix the filtrate, sucrose, agar and dissolve in water filling up to a final volume of 1 liter. Autoclave at 121^0C for 20 min and allow to cool down to 60^0C (Add Blasticidin S to a final concentration of 5 μg/mL for Oatmeal agar/ Blasticidin).

2YEG (Yeast Extract and Glucose)

Yeast Extract	2 g/L
Glucose	10 g/L

Fill up and autoclave at 121^0C for 15 min.

Prune Agar Slant

Prune	4 g/L
Yeast Extract	1 g/L

Lactose	5 g/L
Agar	17 g/L

Fill up, autoclave at 121^{0}C for 20 min, and add Blasticidin S to a final concentration of 5 μg/mL in leaning tubes to obtain slants.

Bottom Agar

Yeast Nitrogen base without amino acid	6.7 g/L
Glucose	5.0 g/L
Sucrose	205 g/L
Agar	15 g/L

Fill up, autoclave at 121^{0}C for 15 min.

Top Agar

Yeast Nitrogen base without amino acid	6.7 g/L
Glucose	5.0 g/L
Agar	10 g/L

Fill up, autoclave at 121^{0}C for 15 min and add Blasticidin S to a final concentration of 5 μg/mL.

Water Agar

Agar	40 g/L

Fill up to 1 liter and autoclave at 121^{0}C for 15 min

Buffers

Sterile Distill water (SDW)

Autoclave distilled water at 121^{0}C for 15 min and allow to cool down at room temperature.

50X Tris Acetic acid EDTA (TAE) Buffer

Tris	242 g
EDTA	18.6 g
Acetic acid	57 mL

Electrophoresis buffer

1 X TAE (200 mL of 50X TAE in 9.8 L of DH_20)

TE buffer

10 mM Tris-Cl, pH 7.5
1 EDTA
Make from 1 M stock of Tris-Cl (pH 7.5) and 500 mM stock of EDTA (pH 8.0).
10 mL 1 M Tris-Cl pH 7.5 per liter.
2mL 500 mM EDTA pH 8.0 per liter.

1M Tris (crystallized free base)

Tris (hydroxymethyl) aminomethane
FW 121.4 g/mol
60.57 g in 0.5 L mq water
pH to 7.5 using HCl

0.5M EDTA

Diaminoethane tetraacetic acid
FW 372.2 g/mol
18.6 g in 100 ml mq water
pH to 8.0 using NaOH
• EDTA Will not be soluble until pH reaches 8.0
• Use vigorous stirring, moderate heat and time

STC Buffer

Sucrose 20%
1M Tris-HCL (1 mL per 100 mL), 10 mM (pH 7.3)
2.5 M $CaCl_2$ (2 mL per 100 mL)
Mix and autoclave at 121^0C for 15 min

Polyethylene glycol (PEG)

PEG 4000 60%
1M Tris-HCL (1 mL per 100 mL), 10 mM (pH 7.3)
2.5 M $CaCl_2$ (2 mL per 100 mL)
Stir and mix while heating

Digestion Buffer Stock

Sucrose (MW: 342) 0.6M (205.5 g/L)
Maleic acid monosodium salt (MMS) ($C_4H_30_4Na.3H_20$), 50 mM (9.65 g/L)
Dissolve MMS in DH_20 and adjust to pH 5.5 before adding sucrose

Working Digestion Buffer (5 mL)

Yatalase 0.1 g
Cellulase 0.025 g
Dissolve in 5 mL of Digestion Buffer Stock.

DEPC-water

Prepared by the addition of 0.l % diethylpyrocarbonate (DEPC, Sigma Chemical Co St. Louis MO, USA) to double-distilled water. The mixture is strongly agitated and left to stand overnight before autoclaving to inactivate the DEPC before use.

Southern Hybridization buffers

Depurination solution (P-Solution)

12NHCl	20 mL
SDW	860 mL

Denaturation solution (D-Solution)

NaCl (An. Grade)	43.83 g
NaOH	10.00 g
SDW	fill up to 1 Liter

Neutralization Solution (N-solution)

NaCl (An. Grade)	43.83 g
Tris (Mwt, 121.14)	30.28 g
SDW	1 Liter

Adjust to pH 7.5 with 12NHCl

20x SSC

Trisodium citrate Dihydrate	88.23 g
NaCl (An. Gnd)	175.3 g
SDW	1 Liter

Adjust to pH 7.0 with I2NHCI

APPENDIX II: DNA DAMAGE AGENTS, ANTIBIOTICS, AND FUNGICIDAL COMPOUNDS USED IN THIS STUDY

Name	Methyl methanesulfonate; MMS
Formula	C2H6O3S
Exact mass	110.0038
Mol weight	110.1322
Structure	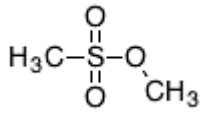

Name	Methyl viologen; Paraquat dichloride; 1,1'-Dimethyl-4,4'-bipyridinium dichloride
Formula	C12H14N2. 2Cl
Exact mass	256.0534
Mol weight	257.159
Structure	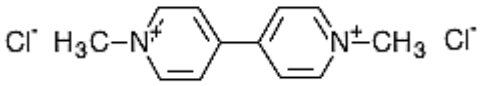

Name	Benomyl; Benlate
Formula	C14H18N4O3
Exact mass	290.1379
Mol weight	290.3177
Structure	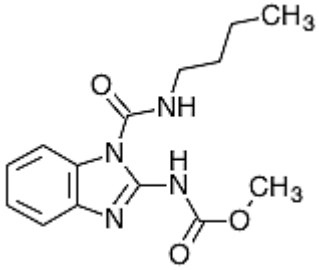

Name	Hydroxyurea; Hydroxycarbamide
Formula	CH4N2O2
Exact mass	76.0273
Mol weight	76.0547
Structure	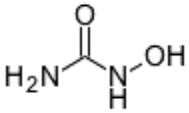

Name	Hydrogen peroxide; H2O2; Oxydol
Formula	H2O2
Exact mass	34.0055
Mol weight	34.0147
Structure	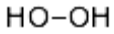

Name	Blasticidin S
Formula	C17H26N8O5
Exact mass	422.2026
Mol weight	422.4389
Structure	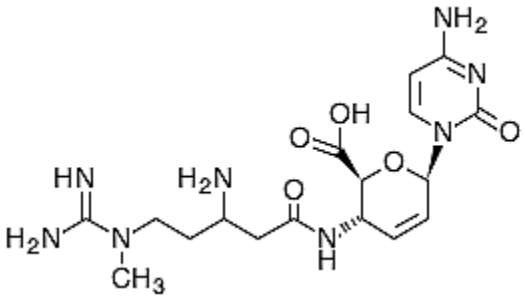

Name	Ampicillin; Anhydrous ampicillin
Formula	C16H19N3O4S
Exact mass	349.1096
Mol weight	349.4048
Structure	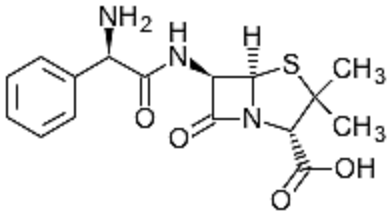

Name	Kanamycin
Formula	C18H33N3O10(R1)(R2)
Structure	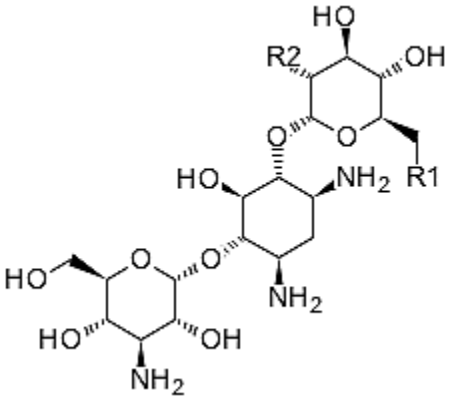

LIST OF ABBREVIATIONS

List of Abbreviations

4NQO	nitroquinoline 1-oxide
Ben	Benomyl
CDK1	Cyclin-Dependent Kinase 1
cDNA	Complementary DNA
Chk2	Checkpoint kinase 2
DAPI	2,4, -Diamidino-phenyl-indole
DNA	Deoxyribonucleic acid
G1	Gap 1
G2	Gap 2
GFP	Green fluorescent protein
HF	High Fidelity
HS	Heat shock
HU	Hydroxyurea
M	Mitosis
MMS	Methyl methanesulfonate
MMS	Methyl methanesulfonate
MV	Methyl viologen
NEB	New England Biolabs
NHEJ	Nonhomologous end-joining
OMA	Oatmeal agar
ORF	Open reading frame
PA	Prune Agar medium
PCR	Polymerase chain reaction
PEG	Polyethylene glycol
qRT-PCR	Quantitative Real-Time polymerase chain reaction
R	Resistant
RNA	Ribonucleic acid
RT-PCR	*Reverse transcription* polymerase chain reaction
SDW	Sterile Distilled *Water*
TE	Tris-HCl EDTA
TEF	Translation Elongation Factor
UV	Ultraviolet
WT	Wild-type
YEG	Yeast extract glucose
Δ	Deletion mutant

Acknowledgements

Acknowledgements

It is of great pleasure to express my sincere and deep gratitude to my advisor and guide Prof. Dr. Teruo Sone, whose expertise, understanding, and generous support made it possible for me to work on a challenging and new topic that was of great interested for me. His enthusiasm for the rice blast kept me continuously engaged with the research, and his personal generously helped make my time at Hokkaido University enjoyable. My special thanks go to Prof. Dr. Satoru Fukiya, Prof. Dr. Norio Kondo and Prof. Dr. Yoshitomo Kikuchi for reading and making the corrections that improved the quality of this thesis.

I owe a deep sense of gratitude to Dr. Abe Ayumi who provided me the best technical guidance during all my experiments. Her prompt guidance, timely suggestions with kindness, and wisdom have enable me to complete my thesis.

My sincere thanks to Prof. Dr. Asano Kozo, Prof. Dr. Yoshitomo Kikuchi, Dr. Souichirou Kato, Dr. Wataru Kitagawa and Prof. Dr. Taichi Takasuka for all comments and suggestions during our weekly seminars. Their advices and scientific approach have helped me to accomplish my tasks.

My gratitude also goes to all students in the Applied Molecular Microbiology laboratory, for their kind help and co-operation.

My appreciation also extends to the Ministry of Education, Culture, Sports, Science, and Technology (MEXT) for supporting my studies at Hokkaido University.

I would like to acknowledge all my friends from several different countries I have made in Sapporo. Our friendship is one of the best things that has happened to me in Japan. Above ground, I indebted to my family and fiancé, who filled me with a life of joy in the hours of difficulties. To all of you I say Thank you very much.